AGU PUBLICATIONS

Geochemistry, Geophysics, Geosystems

RESEARCH ARTICLE
10.1002/2016GC006527

Reconciling mantle wedge thermal structure with arc lava thermobarometric determinations in oceanic subduction zones

Alexander Perrin[1], Saskia Goes[1], Julie Prytulak[1], D. Rhodri Davies[2], Cian Wilson[3], and Stephan Kramer[1]

[1]Department of Earth Science and Engineering, Imperial College London, London, UK, [2]Research School of Earth Sciences, Australian National University, Canberra, Australian Capital Territory, Australia, [3]Lamont-Doherty Earth Observatory, Columbia University, Palisades, New York, USA

Key Points:
- Last equilibration pressures of primitive lavas at oceanic arcs reflect reequilibration within the lithosphere
- Lava equilibration pressures correlate with and span the thickness of the upper plate
- Equilibration temperatures require localized thermal erosion of the lithosphere below the arcs

Supporting Information:
- Supporting Information S1
- Data Set S1

Correspondence to:
A. Perrin,
alexander.perrin09@imperial.ac.uk

Citation:
Perrin, A., S. Goes, J. Prytulak, D. R. Davies, C. Wilson, and S. Kramer (2016), Reconciling mantle wedge thermal structure with arc lava thermobarometric determinations in oceanic subduction zones, *Geochem. Geophys. Geosyst.*, *17*, 4105–4127, doi:10.1002/2016GC006527.

Received 11 JUL 2016
Accepted 29 SEP 2016
Accepted article online 4 OCT 2016
Published online 25 OCT 2016

Abstract Subduction zone mantle wedge temperatures impact plate interaction, melt generation, and chemical recycling. However, it has been challenging to reconcile geophysical and geochemical constraints on wedge thermal structure. Here we chemically determine the equilibration pressures and temperatures of primitive arc lavas from worldwide intraoceanic subduction zones and compare them to kinematically driven thermal wedge models. We find that equilibration pressures are typically located in the lithosphere, starting just below the Moho, and spanning a wide depth range of ~25 km. Equilibration temperatures are high for these depths, averaging ~1300°C. We test for correlations with subduction parameters and find that equilibration pressures correlate with upper plate age, indicating overriding lithosphere thickness plays a role in magma equilibration. We suggest that most, if not all, thermobarometric pressure and temperature conditions reflect magmatic reequilibration at a mechanical boundary, rather than reflecting the conditions of major melt generation. The magma reequilibration conditions are difficult to reconcile, to a first order, with any of the conditions predicted by our dynamic models, with the exception of subduction zones with very young, thin upper plates. For most zones, a mechanism for substantially thinning the overriding plate is required. Most likely thinning is localized below the arc, as kinematic thinning above the wedge corner would lead to a hot fore arc, incompatible with fore-arc surface heat flow and seismic properties. Localized subarc thermal erosion is consistent with seismic imaging and exhumed arc structures. Furthermore, such thermal erosion can serve as a weakness zone and affect subsequent plate evolution.

1. Introduction

Subduction zones are the location of the greatest mass and heat fluxes at Earth's surface and, thus, are critical to understanding a wide array of Earth processes. For example, subduction exerts primary control on ore-deposit formation [e.g., *Sillitoe*, 2010; *Wilkinson*, 2013], the generation and growth of continental crust [*Huene and Scholl*, 1991; *Taylor and McLennan*, 1995], and the cycling of volatiles [e.g., *van Keken et al*., 2011; *Peacock*, 1990]. The mantle wedge is a key part of the subduction system, where magmas are generated and transferred to the arc, likely instigated by volatile release from the downgoing plate [*Tatsumi*, 1986; *Schmidt and Poli*, 1998; *Grove et al*., 2012; *Gill*, 2012]. Furthermore, the mantle wedge plays a key role in the dynamic plate-mantle interaction and plate coupling [e.g., *Billen and Gurnis*, 2001; *Arcay*, 2012].

Magma genesis, transport and the position of the arc are affected by (Figure 1): (a) subducting plate conditions, (b) mantle wedge conditions, and (c) the upper plate. The relative importance of each of these factors remains debated, with geochemical and geophysical studies providing independent constraints that support various scenarios. We next discuss these constraints, in turn.

a. The thermal conditions of the subducting plate are critical in considering the link between arc volcanism and slab dehydration [e.g., *Tatsumi*, 1986; *Grove et al*., 2002]. The variation of slab temperatures with depth (i.e., with pressure) controls where dehydration reactions occur [*Schmidt and Poli*, 1998; *van Keken et al*., 2011]. The so-called thermal parameter, Φ, captures the slab temperature as a function of depth through the product of age, A, and subduction velocity, V_c, and dip, δ, of the subducting plate, $\Phi = A\ V_c \sin\delta$ [*McKenzie*, 1969; *Syracuse et al*., 2010]. This, in turn, provides the boundary condition for where volatile-induced magma genesis in the overlying wedge is possible [*Gaetani et al*., 1993; *Schmidt and Poli*, 1998].

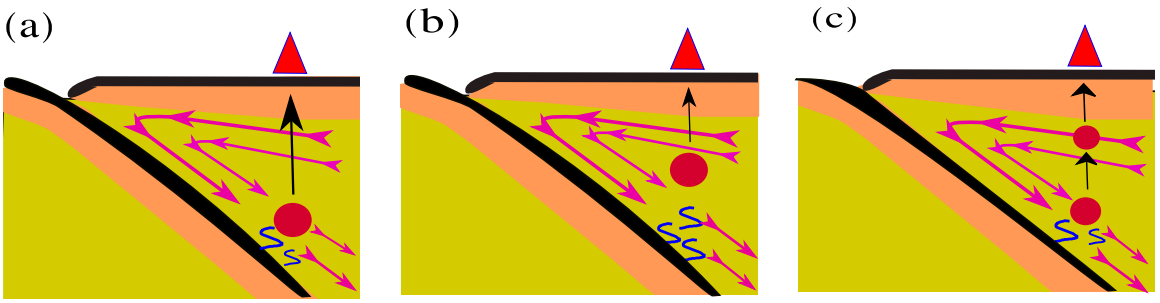

Figure 1. Cartoon of corner flow within the mantle wedge, and possible locations of melt generation and equilibration. Pink lines show the flow paths of the mantle within the wedge, typical of the "corner flow" mechanism that is thought to be driven by the subducting plate. Mantle is drawn into the corner and erodes the lithosphere of the upper plate. Blue lines indicate fluid released from the slab/mantle that rises into the wedge. Red circles indicate the locations of melt generation or equilibration. Black arrows are the flow paths of the melt. Red triangles indicate the volcanic front. (a) Main magma generation near the slab surface, and subsequent rise to the volcanoes. (b) Main magma generation within the center of the wedge, and subsequent rise to the volcano. Figure 1c shows magma generation within the wedge, by either Figure 1a or Figure 1b, but with subsequent reequilibration with mantle during ascent. We use the following terminology in this scenario. The "source" is the mantle from which the magma initially forms. The "residue" is the source postmelting. The "host" is the mantle with which the magma last reequilibrated.

Recent experimental studies on subducting sediment and slab compositions have proposed a suite of chemical "geothermometers" which are designed to estimate subarc slab surface temperatures. In essence, geothermometers use the solubility of an accessory phase containing trace elements of interest as major structural components (e.g., Ce in allanite) to determine the temperature of the fluid coexisting with the accessory phase. *Hermann and Spandler* [2007] suggested the use of K_2O/H_2O, while *Klimm et al.* [2008] suggested the use of LREE/Ti. *Plank et al.* [2009] provided a review of geothermometers and advocated the use of H_2O/Ce in particular. *Cooper et al.* [2012] then used the H_2O/Ce geothermometer and found a positive correlation of temperature estimates determined from H_2O/Ce ratios measured in melt inclusions in primitive olivine from global subduction zones to slab surface temperatures derived from the numerical models of *Syracuse et al.* [2010]. This relationship suggests that the thermal state of the slab may be reflected in the composition of fluids released from the slab into the wedge and that the erupted magmas may "remember" this signature.

Turner and Langmuir [2015a] compiled a global database of primitive arc magma chemistry, including major elements, trace elements, and radiogenic isotopes. They confirmed the original observations of *Plank and Langmuir* [1988] that sodium and calcium contents of magmas normalized to 6 wt % MgO correlate with the thickness of the arc crust. *Turner and Langmuir* [2015b] extended the major element findings to suggest trace element ratio correlations (e.g., La/Yb and Zr/Ti) with crustal thickness as well as, arguably, the slab thermal parameter. Although *Turner and Langmuir* [2015b] prefer a model where the mantle wedge provides the dominant control, they were also able to recreate the chemical correlations with a model where the chemistry of the erupted magmas is controlled by slab thermal structure and its effect on the release of slab components. However, critically, they find that their chemical trends do not correlate with slab temperatures predicted by thermal models at the depth directly below the arc [*Syracuse et al.*, 2010]. Thus, it appears that although the slab controls fluid input into the mantle wedge, it may not be the main controlling factor for melt major and trace element composition and migration pathways [e.g., *Grove et al.*, 2012; *Schmidt and Poli*, 2014; *Turner et al.*, 2016].

b. Mantle wedge conditions likely influence how melts rise. One end-member model is that melt migrates as a fully distributed and reactive flux, for which the thermal conditions determine whether the melt reaches the upper plate before freezing [*Grove et al.*, 2002, 2012]. Alternatively, more focused melt pathways (or those of the released fluids that lead to melting) may be the result of a balance between the mantle wedge's flow regime, and resistance to melt ascent by permeability variations, which arise through thermally controlled variations in viscosity and compaction [*Spiegelman and McKenzie*, 1987; *Sparks and Parmentier*, 1991; *Cagnioncle et al.*, 2007; *Wilson et al.*, 2014]. Finally, it has been suggested that melts may rise in diapirs [*Bremond d'Ars et al.*, 1995; *Hall and Kincaid*, 2001], which may contain metamorphic melange mixtures of low-density subducted components (sediments and hydrous crustal material), hydrated mantle, and melts [e.g., *Gerya and Yuen*, 2003; *Behn et al.*, 2011; *Marschall and Schumacher*, 2012].

The wedge is likely to be the dominant location of melt formation. Several studies that compared pressure (P) and temperature (T) conditions inferred from melt inclusions with indicators of melt fraction are

in general agreement that the derived P and T reflect primary melting conditions [*Kelley et al*., 2010; *Watt et al*., 2013]. These P, T conditions commonly correspond to the shallow wedge. In particular, the wedge corner has been suggested as a location for melt formation, because the upper plate may be easily eroded due to the strain associated with the turning flow [e.g., *Kelemen et al*., 2003].

Turner and Langmuir's [2015b] preferred model is one where melt compositions are primarily controlled by mantle wedge conditions. They proposed that arc crustal thickness (the subduction parameter with which they found their strongest trends) is positively correlated with upper plate lithospheric thickness and, accordingly, wedge thermal structure and the depth range of melting. This model predicts a fourfold difference in degree of melting, and consequently a fourfold primary meltwater content difference, in subduction zones worldwide.

The mantle wedge's thermal structure has also been proposed as a first-order control on the position of the volcanic arc front [*England and Katz*, 2010; *Grove et al*., 2009]. *Grove et al*. [2009] proposed that the stability field of hydrous minerals (particularly chlorite) in the slab and mantle wedge largely control where the arc forms, over a region that may span several 100 km from the wedge corner toward the back arc. *England and Katz* [2010] suggested that the region where anhydrous melting is possible in the wedge may control the focusing of volcanism along a narrow arc. According to their analytical models [*England and Wilkins*, 2004], wedge temperatures depend on a product of subduction velocity and the sine of slab dip, $V_c \sin\delta$. When *Turner and Langmuir* [2015b] add a dependence of magma composition on $V_c \sin\delta$ into their wedge models, this further improves data confluence. In contrast, including slab age does not lead to improvements in data matching. Thus, there is both geochemical and geophysical evidence that mantle wedge pressure-temperature conditions may exert an important control on magma generation and transport.

c. Finally, it is important to consider the effect of the upper plate on mantle wedge thermal structure. In detail, *Turner and Langmuir* [2015b] infer that the upper plate controls wedge structure and thereby melting conditions. In numerical models of thermal wedge structure there is a feedback between overriding plate structure and wedge flow, where overriding plate thickness puts a constraint on underlying wedge flow, but wedge flow can also erode the upper plate's thermal boundary layer thus thinning it, particularly in the wedge corner [e.g., *Kelemen et al*., 2003; *Arcay et al*., 2005; *Conder*, 2005]. *England and Katz* [2010] propose that it is this interplay which leads to the focusing of melting below the arc. In their model, the enhanced thinning of the upper plate above the wedge corner provides the location where wedge conditions approach the dry solidus and hence the extent of melting is highest. They propose that above this highest melt region, localized thermal erosion of the upper plate occurs to form the arc [*England and Katz*, 2010]. Others have suggested that upper plate stress state may in some zones (e.g., Sumatra) exert the dominant control on arc position, which would hence be independent of wedge structure [*Pacey et al*., 2013; *Schmidt and Poli*, 2014].

A number of previous studies have investigated the generation and transport of melts at arcs using the equilibration P, T conditions of primitive subduction zone melts. Most have yielded relatively high (mantle wedge like) T (1200–1400°C) at low P (around 1 GPa), which is close to the Moho for continental arcs (see compilation of data by *Kelemen et al*. [2003]), although some studies, in particular those using melt inclusions [e.g., *Kelley et al*., 2010; *Plank and Forsyth*, 2016], obtained similarly high temperatures at elevated pressures (2–4 GPa). A number of different interpretations have been proposed: (1) the high temperatures reflect transient conditions associated with melts rising from the wedge [*Elkins-Tanton et al*., 2001; *Ruscitto et al*., 2010]; (2) the P, T conditions correspond to the wedge corner above which the overriding plate has been substantially thinned by corner flow [*Kelemen et al*., 2003; *Grove et al*., 2012]; and (3) local thermal modification of the lithosphere below the arc was suggested, similar to the model of *England and Katz* [2010], in order to reconcile petrological and geodynamical constraints for the conditions obtained from two samples in the Aleutians and Mexico [*Weaver et al*., 2011].

Here we perform a global compilation of pressure and temperature conditions from major element thermobarometry of primitive mantle melts from intraoceanic subduction zones and compare these conditions with our subduction zone thermal models. We explore whether: (a) primitive melt P, T conditions agree with wedge melting conditions in a global sense and (b) if P, T conditions correlate with any physical subduction parameters that may provide insight to whether the subducting slab, the upper plate or mantle wedge's thermal structure is the dominant control on magma generation and transport.

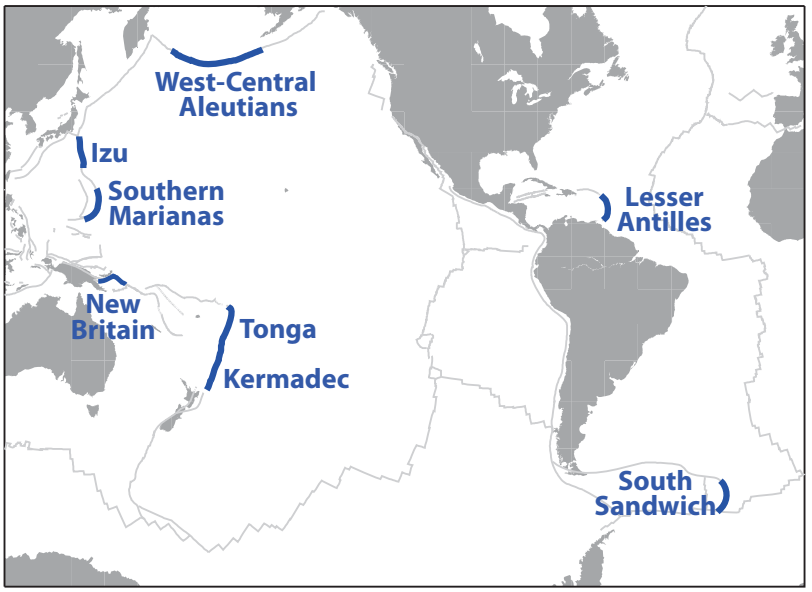

Figure 2. Map of the intraoceanic trenches studied (in blue). Plate boundaries in light gray.

2. Method

We focus on well characterized intraoceanic arcs (as defined in *Syracuse et al*. [2010]), with simple oceanic upper plates (Figure 2), to avoid complications arising from possible crustal contamination by thick continental crust. These are Izu, Southern Marianas, Tonga, Kermadec, New Britain, the Lesser Antilles, and South Sandwich. We also include the West-Central Aleutians, which is considered to be largely oceanic. Other ocean-ocean arcs, the Phillipines, Vanuatu, New Zealand, and Calabria, were not considered due to their complex tectonic history and/or partly continental upper plates.

For each of these zones, we use two independent methods for determining mantle P, T conditions below the arcs. The first (section 2.1) uses whole-rock major element chemistry of arc lavas and applies the thermobarometer developed by *Lee et al*. [2009] to obtain the P, T conditions of last equilibration with the mantle. The second (section 2.2) employs kinematic numerical models, following the approach of *Syracuse et al*. [2010] and *Le Voci et al*. [2014] to predict thermal structures for each of the subduction zones from which the chemical data are obtained.

2.1. Thermobarometry

2.1.1. Arc Database

Arc lava compositions were compiled from the GEOROC database (http://georoc.mpchmainz.gwdg.de/georoc/). Because the thermobarometric calculation of *Lee et al*. [2009] is dependent on the major element composition of the lavas, we choose to examine samples with MgO contents between 6 and 10 wt %, rather than compare those at a similar stage in their fractionation history (e.g., 6 wt % MgO), which is more appropriate for evaluating broad differences in the trace element chemistry of magmatic sources [e.g., *Turner and Langmuir*, 2015a]. The lower bound of 6 wt % is to exclude lavas that have undergone extensive crystal fractionation, while the upper bound is to remove magmas that have likely accumulated mafic phases. We would ideally have set the lower bound higher (e.g., 8 wt % MgO), but lavas in subduction zones are more fractionated than in other tectonic settings, leading to a paucity of lavas with 8–10 wt % MgO. Data were next individually analyzed for each subduction zone, to include only samples from the active arc front and exclude back arc, fore arc, and older lavas for which the current geometry of the subduction zone is not applicable. Major and trace element geochemistry of lavas with 6–10 wt % was further scrutinized and samples with a clear plume influence (e.g., Niuatoputapu, Tonga) were also excluded. We also excluded any samples from studies predating 1975 (as in *Turner and Langmuir* [2015a]), and only those whose the major elements had been analyzed by XRF or EMPA on glass, to ensure accurate SiO_2 contents. The database is

included as Supporting Information. We compared with the database compiled by *Turner and Langmuir* [2015a] to test robustness of the results.

2.1.2. Thermobarometric Method

We apply the major element thermobarometer proposed by *Lee et al*. [2009] to our filtered database of arc lava geochemistry. This thermobarometer has been used in the study of lava equilibration pressures and temperatures across a range of tectonic settings, including subduction zones [*Watt et al*., 2013; *Kelley et al*., 2010; *Weaver et al*., 2011; *Mullen and Weis*, 2015], back arcs [*Kelley et al*., 2010; *Lytle et al*., 2012], the basin and range province [*Plank and Forsyth*, 2016], and mantle plumes [*Konter and Becker*, 2012].

An individual pressure and temperature condition for a lava sample is calculated as follows. The major element composition of a lava is specified, along with the primary H_2O content, mantle $Fe^{3+}/\Sigma Fe$, and host Mg#. It is assumed that the lava has undergone some olivine fractionation between the point it last equilibrated with the mantle and eruption. Olivine is added back to the composition, until the Mg# of the lava is in equilibrium with its assumed host mantle. When the primary magma composition has been estimated, the activity of SiO_2 in the primary melt, which is sensitive to the equilibration pressure, is calculated. Temperatures are estimated based on Fe-Mg exchange, taking into account the effect of the specified water content [*Lee et al*., 2009].

The thermobarometer requires olivine and orthopyroxene to be multiply saturated in the magma source region [*Lee et al*., 2009], which is a reasonable assumption in subduction zones, where the source is likely to be modally similar to a depleted MORB mantle (DMM). The thermobarometer was calibrated using a large experimental database of basaltic liquids over pressures up to 7 GPa and temperatures of 1100–1800°C. Uncertainties in P and T were estimated to be $\pm$0.2 GPa, and 30–50°, respectively. Similar uncertainties were confirmed in a detailed experimental study of two lavas, one from the Aleutian and one from the Mexican volcanic arcs [*Weaver et al*., 2011]. *Abers et al*. [2014] found that the *Lee et al*. [2009] thermobarometer yielded temperature estimates that agreed within a few tens of degrees with estimates using Fe_8 and Na_8.

2.2. Numerical Model Setup

For each of the seven chosen subduction zones, we use plate geometry and velocities from *Syracuse et al*. [2010] to define a kinematically prescribed subducting plate. We then solve numerically for the consequent flow to a depth of 400 km in the overlying mantle wedge and below the subducting plate, as well as for temperature throughout the whole domain. The Stokes and energy equations, assuming an incompressible Bousinessq formulation, are solved using the finite element, control-volume code fluidity [*Davies et al*., 2011; *Kramer et al*., 2012]. Full details of the methods as well as the reproduction of kinematic subduction benchmarks of *van Keken et al*. [2008] can be found in *Le Voci et al*. [2014] and *Davies et al*. [2016].

The model setup is similar to that of the models examined by *Syracuse et al*. [2010] (Figure 3). The top 10 km of the subducting plate is set to the velocity of the subducting slab. As the subducting slab is cold and viscous, this top layer drags the rest of the slab that resides beneath it. The upper plate is given a zero velocity down to a depth of 50 km in our reference setup (smaller depths are tested in a few cases). We also set velocities to zero in a small region below this fixed upper plate thickness, over a region 5 km thick directly above the subducting slab. This allows us to prescribe the depth to which full decoupling between the slab and upper plate persists. Several previous studies [*Wada and Wang*, 2009; *Syracuse et al*., 2010] preferred a decoupling depth of around 80 km as this leads to the formation of a cool fore-arc corner, most consistent with observations of low fore-arc surface heat flow and imaged seismic velocities and attenuation of the fore-arc mantle [e.g., *Kincaid and Sacks*, 1997; *Hyndman and Peacock*, 2003; *Currie and Hyndman*, 2006; *Rychert et al*., 2008]. However, others preferred shallower depths [*Kelemen et al*., 2003] or depths that evolved in response to thermal structure [*Arcay et al*., 2005; *Arcay*, 2012]. Our default decoupling depth is 80 km, but as decoupling depth is one of the key parameters controlling wedge temperatures, we will discuss how varying this depth affects thermal structure and compatibility between the thermal models and the thermobarometric data.

Other mechanical boundary conditions imposed are stress-free sides below the two kinematically prescribed plates, as well as a stress-free base below the subducting plate. At the base of the model above the slab, an outflow velocity equal to that of the subducting plate is applied, to simulate the effect of the deeper slab [see *Le Voci et al*., 2014]. This boundary always extends 100 km to the right of the slab, and therefore the entire width of the model varies depending on the dip of the slab in each case, extending

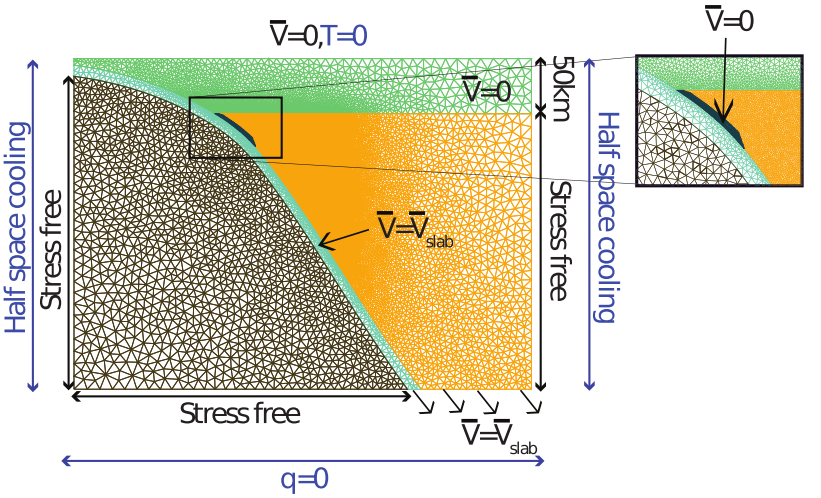

Figure 3. Model setup showing the grid used, color-coded according to the velocity conditions prescribed, and the boundary conditions applied. Velocities are prescribed in the top 10 km of the slab (cyan) and top 50 km of the upper plate (green), while they are solved for in the wedge (orange) and below the slab (black). The geometry of the subducting plates is based on the analysis of *Syracuse and Abers* [2006]. We model the decoupling depth by prescribing a thin region (black area shown in inset, ~5 km thick) of zero velocity above the slab. This extends to 80 km depth.

between 300 and 500 km oceanward from the trench. Temperature boundary conditions are 273 K on the top, an error function commensurate with the incoming and overriding plate ages on the side, and zero heatflux on the bottom boundary. Mantle potential temperature is set to 1350°C [*Courtier et al*., 2007], although a hotter temperature of 1421°C used by *Syracuse et al*. [2010] based on the plate model of *Stein and Stein* [1992] was also examined.

We assume a temperature, pressure, H_2O-dependent composite diffusion- and dislocation-creep rheology, with the same parameters as *Davies et al*. [2016], for a damp mantle with a hydration of 1000 H/10^6Si (Table S1). All material parameters are as in *Le Voci et al*. [2014] and summarized in Table S1.

The initial temperature field is set to an error function according to the chosen downgoing and initial upper plate ages in the plates, and mantle potential temperature below. They are then run until the upper plate reaches the thermal age as given in the *Syracuse et al*. [2010] database. The initial upper plate age is chosen to allow the thermal structure of the downgoing plate to reach a quasi steady state. For example, in Tonga, to take a snapshot at the current upper plate age, we set the initial upper plate thermal structure according to a half-space cooling model with an age of 1 Myr. The model is then run and a snapshot of the thermal structure is taken at 9 Myr, to provide an approximation of the 10 Myr upper plate age. The plate reaches the base of the model after 2 Myr, and subsequently slab thermal structure stabilizes for another 7 Myr. Where the upper plate is very young, for example in New Britain where the age is 2 Myr [*Syracuse et al*., 2010], there is insufficient time for the thermal structure to develop and so we take a snapshot of the thermal structure at 8 Myr.

Other studies have preferred to analyze models when the wedge reaches a (quasi)steady state [e.g., *Syracuse et al*., 2010]. *Kelemen et al*. [2003] report that time to steady state in their wedge models is 10 Myr for the wedge corner and 100 Myr for the entire model, while *Dumoulin et al*. [2001] found similarly long time scales for oceanic lithosphere to achieve a thermal equilibrium, i.e., time scales that exceed the age of many of the Pacific subduction zones. *Syracuse et al*. [2010] run their models for 20 Myr to approximate a steady state velocity field and then solve for the corresponding temperatures. Given the notably high temperatures at low pressures often obtained from thermobarometry, considering a snapshot of the thermal structure at a time equal to the upper plate age rather than letting the upper plate cool to a steady state, increases the likelihood of reconciling thermal models and thermobarometric data. Furthermore, as summarized by *Schmidt and Poli* [2014], subduction zones are generally not in a steady state, as suggested by the lack of correlation between the parameters governing the thermal field within the wedge and the position of the arc.

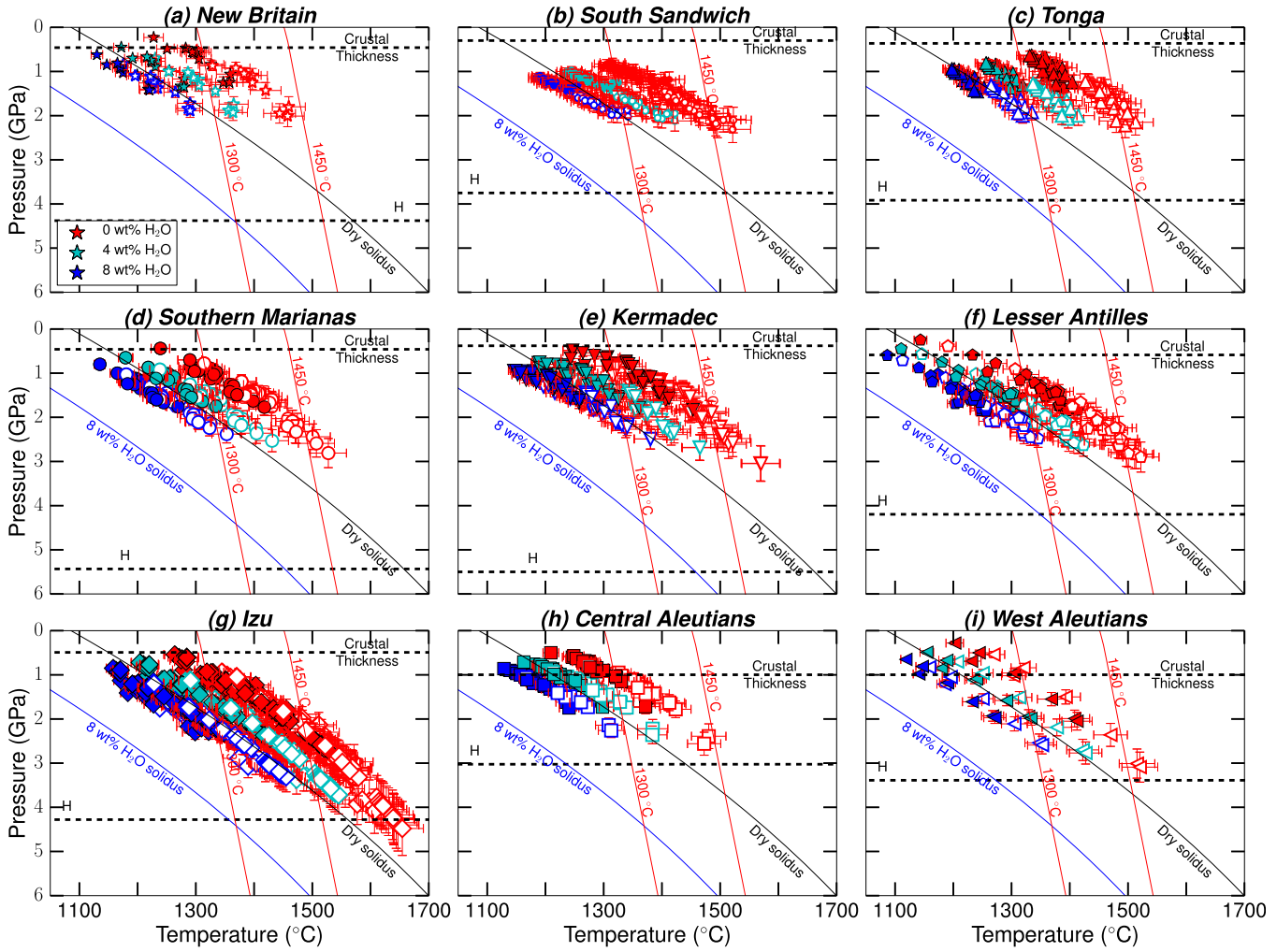

Figure 4. Calculated magma equilibration *P*, *T* using the thermobarometer of *Lee et al*. [2009] for all arcs, in order of upper plate age, exploring uncertainty in primary melt H_2O content (from 0 (red) to 8 (blue) wt %), Mg# of the host rock (filled symbol = 0.9, hollow = 0.92), and fO_2 (0.1–0.2 as shown by red error bars, points plotted at 0.15). Each point represents the calculated *P*, *T* for one lava sample. For example, for the Tonga data set, the red filled symbols represent the *P*, *T* for all the lavas from the data set calculated assuming primary H_2O = 0 wt %, host Mg# = 0.9, and fO_2 = 0.15. The hollow symbols are the calculated *P*, *T* of the data set, assuming the same parameters, except for host Mg# = 0.92. For comparison, we plot solidi from *Katz et al*. [2003], crustal thicknesses from *Clift and Vannucchi* [2004], and slab surface depths below the arc, marked by an H, from *Syracuse et al*. [2010]. Red lines are adiabats for potential temperatures of 1350 and 1450°C.

3. Results: Major-Element Thermobarometry

3.1. Uncertainties in Thermobarometric Calculations

Figure 4 shows the thermobarometric P, T estimates obtained from filtered samples for all arcs in our database. We first discuss the sensitivity of calculated pressure and temperature to host rock composition (i.e., Mg#), primary H_2O content, and oxygen fugacity.

3.1.1. Effect of Magmatic Evolution

The thermobarometer corrects only for olivine fractionation, and thus fractionation of other phases could affect the calculated primary major element composition and subsequent pressure and temperature estimates. *Lee et al*. [2009] choose samples with >8.5 wt % MgO, to ensure that only olivine has fractionated. Arc lavas are typically more fractionated than those from other tectonic settings and, as noted previously, choosing this minimum MgO would dramatically reduce the number of the samples available for analysis. A plot of equilibration pressure versus MgO for all MgO contents yields some sense of lower MgO lavas tending to have lower calculated pressures in some subduction zones (Figure S1). However, this trend is most pronounced in lavas with MgO <6 wt %. Although this uncertainty is likely negated by our filtering criteria,

Table 1. Effect of Altering H_2O Content, Host Mg#, or $Fe^{3+}/\Sigma Fe$ on Selected Samples From Tonga (Chosen to Cover a Range of P, T Space)[a]

Changing H_2O Content From 0 to 8 wt % Host Mg# = 0.91, $Fe^{3+}/\Sigma Fe = 0.15$				
Sample Name	Ave. P (GPa)	P_0–P_8 (GPa)	Ave. T (°C)	T_0–T_8 (°C)
89T25	1	−0.2	1306	148
T052A	1.3	−0.1	1324	150
482-8-11	1.7	0	1357	162
Average	1.3	−0.1	1329	153
Altering Host Mg# From 0.90 to 0.92 H_2O Content 4 wt %, $Fe^{3+}/\Sigma Fe = 0.15$				
Sample Name	Ave. P (GPa)	$P_{0.92}$–$P_{0.90}$ (GPa)	Ave. T (°C)	$T_{0.92}$–$T_{0.90}$ (°C)
89T25	1.1	0.5	1301	82
T052A	1.4	0.5	1319	85
482-8-11	1.7	0.7	1352	91
Average	1.4	0.6	1324	86
Altering $Fe^{3+}/\Sigma Fe$ From 0.1 to 0.2 Host Mg# = 0.91, H_2O Content 4 wt %				
Sample Name	Ave. P (GPa)	$P_{0.1}$–$P_{0.2}$ (GPa)	Ave. T (°C)	$T_{0.1}$–$T_{0.2}$ (°C)
89T25	1	0.2	1297	42
T052A	1.3	0.3	1316	44
482-8-11	1.7	0.3	1348	47
Average	1.4	0.3	1320	44

[a]Uncertainties generally increase with increasing P and T.

it is of interest to assess the magnitude of calculated pressure and temperature change induced by unaccounted crystal fractionation.

To ensure olivine only fractionation, *Abers et al*. [2014] based their sample choice on MgO-CaO and MgO-Al_2O_3 relationships, and this results in the inclusion of samples with <6 wt % MgO. The effects of ignoring possible plagioclase and clinopyroxene fractionation were considered. Plagioclase fractionation caused a slight overestimate of SiO_2 and MgO [*Lee et al*., 2009], leading to a slight overestimate of T and P. However, in water rich magmas typical of subduction zones, plagioclase crystallization is suppressed [e.g., *Gaetani et al*., 1993], thus our filtering criteria of 6–10 wt % MgO makes it unlikely that our samples are affected by this process. Ignoring clinopyroxene (cpx) fractionation results in an underestimate of SiO_2 and an overestimate of MgO, resulting in a lower P and higher T estimate. *Abers et al*. [2014] quantified the effects of cpx fractionation by adding back cpx until the magma had 12 wt % CaO. Their cpx correction resulted in a temperature decrease of 10°C and a pressure decrease of 0.05 GPa. Overall, a generous estimate of the uncertainty resulting from unaccounted fractionation of plagioclase and clinopyroxene in our filtered lavas is on the order of (10°C and 0.05 GPa, i.e., ~2 km) and does not impact our interpretations.

3.1.2. Effect of fO_2

When magma composition is corrected for olivine fractionation, a partition coefficient dependent on the Fe^{2+} concentration and Mg# of the melt and mantle is used. This calculation is dependent upon the relative amount of Fe^{2+} to Fe^{3+} in the primary magma ($Fe^{3+}/\Sigma Fe$). The original $Fe^{3+}/\Sigma Fe$ is uncertain as the oxidation state of the mantle is strongly debated [e.g., *Kelley and Cottrell*, 2009; *Lee et al*., 2010]. *Kelley and Cottrell* [2009] suggest that the magmatic $Fe^{3+}/\Sigma Fe$ of subduction zones is more oxidized, with values in the region of 0.18–0.32 (compared with 0.13–0.17 at ridges and 0.15–0.19 at back arcs). *Lee et al*. [2005, 2010] have advocated negligible difference in the oxidation state of the mantle beneath volcanic arcs and mid-ocean ridges, and thus employed a value of 0.1 in their analysis of subduction zone lavas in *Lee et al*. [2009]. *Abers et al*. [2014] select specific values of $Fe^{3+}/\Sigma Fe$ for each of the arcs they consider. For example, in the Marianas, a value was selected for individual islands (ranging from 0.23 to 0.26) based on available data. In Costa Rica and Nicaragua, where there is no available data, *Abers et al*. [2014] assume a ratio of 0.25. *Kelley et al*. [2010] assume a value of 0.25 for the Mariana arc. All else being equal, increasing $Fe^{3+}/\Sigma Fe$ to more oxidizing conditions results in a decrease in estimated pressure and temperature (see Table 1). The symbols in Figure 4 are calculated with $Fe^{3+}/\Sigma Fe = 0.15$, with error bars depicting calculations at $Fe^{3+}/\Sigma Fe = 0.1$ and

0.2. As the effect is relatively small (on the order of 0.2–0.3 GPa), and the oxidation state of subduction zone mantle is an area of much debate, we choose to set $Fe^{3+}/\Sigma Fe$ to 0.15 for all samples.

3.1.3. Effect of Changes in Primary H_2O Content

Primary H_2O contents of subduction zone magmas are thought to vary from dry (<1 wt %) to wet (>8 wt %) [*Grove et al*., 2002] (Figure 4). From worldwide melt inclusion data, however, the primary H_2O concentrations are thought to be on average 4 wt % [*Plank et al*., 2013], which we assume when comparing models. The effect of H_2O variation on equilibration conditions is shown in Table 1. Decreasing the assumed H_2O content has a relatively small effect on pressure. For a large water content variation from 8 to 0 wt %, pressure estimates change by up to −0.3 GPa for the lowest pressures [see also *Lee et al*., 2009] to less than −0.1 GPa for pressures above 1 GPa. The effect on temperature estimates is more substantial and a decrease in water content from wet to dry increases the temperature by around 150°.

3.1.4. Effect of "Host" Composition

The Mg# (where Mg# = Mg/(Mg+Fe)) of the mantle "host" with which the magma last equilibrated is an unknown variable linked to the melt depletion history of the mantle source, with progressive depletion resulting in higher Mg#. For example, many studies suggest that the mantle wedge is more depleted than the source of MORB, perhaps due to melt depletion in the back arc [*McCulloch and Gamble*, 1991; *Woodhead et al*., 1993; *Kimura and Yoshida*, 2006]. The DMM1 composition [*Wasylenki et al*., 2003] which is equivalent to the depleted MORB mantle (DMM) with 10% melt removed, has Mg# ∼0.9. Given that it is highly unlikely that arc lavas derive from a source with Mg# <0.9, *Lee et al*. [2009] initially explored a range of 0.9–0.92 for subduction zones. Progressive host depletion as reflected in changing Mg# from 0.90 to 0.92 results in significantly higher calculated pressures (∼0.5–0.7 GPa) and elevated temperatures (∼80–90°C) (Figure 4 and Table 1). *Abers et al*. [2014] assume a host Mg# of 0.9 for all three subduction zones they consider, but give little justification. *Weaver et al*. [2011] use SiO_2 and TiO_2 contents of oceanic arc magmas from five subduction zones to argue that lavas from oceanic arcs equilibrate more often with a lherzolitic host rock (Mg# = 0.9). Harzburgitic hosts (i.e., Mg# > 0.9) are possible, but more common in continental margin arcs. Given this uncertainty and previous work, we assume Mg# = 0.9 as our reference value, but explore the effect of using more depleted host compositions.

3.1.5. Summary

Overall, temperature estimates are most sensitive to primary H_2O content, while host Mg#, fO_2, and magmatic evolution (in order of importance) play a secondary role. In contrast, pressure is most affected by the choice of host Mg#, with less sensitivity to fO_2, H_2O, and magmatic evolution.

3.2. Calculated Pressures and Temperatures

3.2.1. Inferred P and T Ranges

While the range and average pressures vary in each subduction zone, a few distinct global characteristics stand out, irrespective of the uncertainties discussed above. These are illustrated in Figure 4, by focusing on a set of pressure and temperature conditions with a single host rock composition (e.g., solid symbols) and 4 wt % water (e.g., cyan symbols).

1. Most thermobarometric conditions lie at relatively low pressures which fall in a lithospheric depth range from the Moho to 100 km depth, with an average for all zones of about 40 km depth.
2. A large range of pressures is obtained for each subduction zone (especially for Izu, where they span >2 GPa, i.e., over 60 km). For all zones, the average pressure range is ∼0.8 GPa, corresponding to about 25 km.
3. Relatively high temperatures are obtained at shallow depths, all near the temperatures of a dry solidus. These temperatures are more like those expected in the central region of the mantle wedge, rather than those of a conductive lithosphere.
4. Compared to the range of temperatures expected in the upper plate and mantle wedge (from close to surface temperatures near 0°C to wedge temperatures of around 1350°C), for a constant water content, the range of temperatures is narrow, generally only spanning 100–200°C.
5. For a constant water content, the P, T conditions approximately parallel the solidi, i.e., a trend steeper than a conductive lithospheric geotherm, but less steep than either a mantle or a melt adiabat. This is most apparent for the subduction zones where points span the largest pressure ranges (e.g., Figure 4g). This implies that the apparent degree of melting is relatively constant over the range of P, T conditions in each zone. The geotherms defined by the P, T data are similar to those that are predicted from adiabatic melting models [e.g., *Morgan*, 2001], where latent heat extraction by melting leads to increasingly

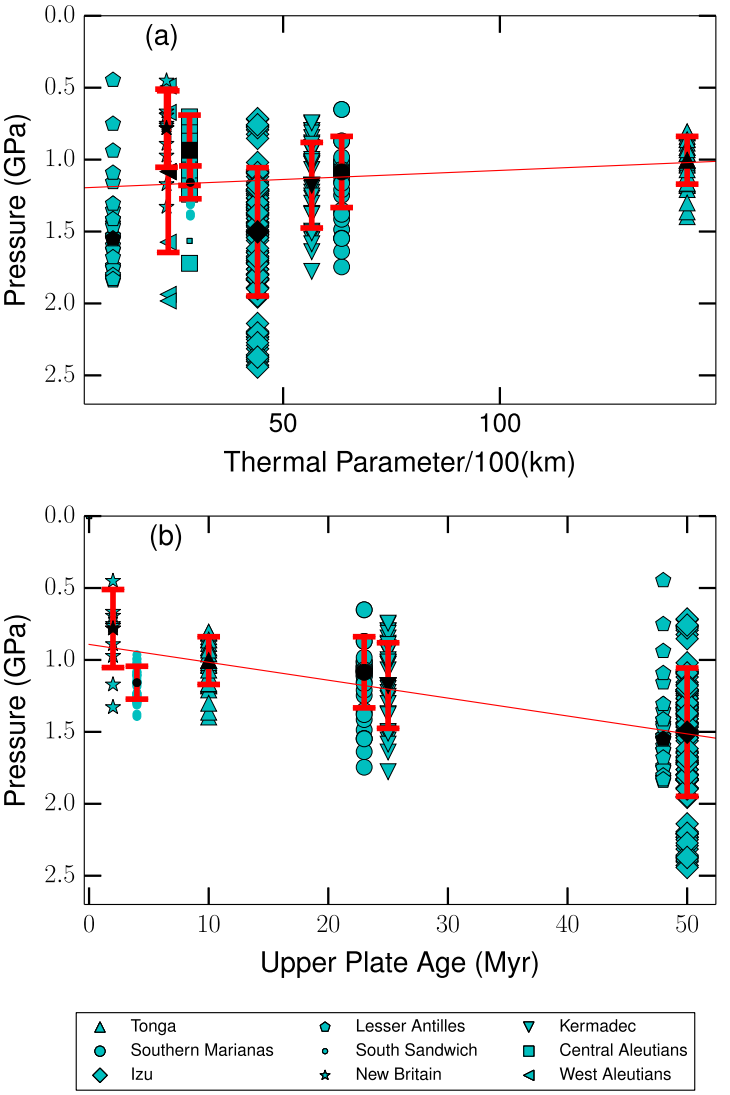

Figure 5. Pressure estimations assuming H_2O content = 4 wt %, host Mg# = 0.9, Fe^{3+}/Fe_{total} = 0.15 versus (a) arc thermal parameter and (b) upper plate age. Each cyan point is an individual sample pressure. Black markers are medians, and red error bars are standard deviations for each arc data set. Note that the Lesser Antilles actually has an upper plate age of 50 Ma, but has been offset slightly to enable clearer viewing of data. The same is true for the Southern Marianas (actual 25 Myr upper plate age) and South Sandwich (actual 2 Myr upper plate age). While there is a poor correlation between the thermal parameter and various parameters of the P distribution (with mean: r = 0.25, median: r = 0.20, standard deviation: r = 0.38, range: r = 0.40), there is a good correlation of P with upper plate age (with mean: r = 0.91, median: r = 0.89, standard deviation: r = 0.83, range: r = 0.91).

subadiabatic temperatures, along trends close to that of the solidus, as initially adiabatic mantle rises to shallower depths.

3.2.2. Trends With Subduction Parameters

Next we examine the covariation of calculated P and T with a range of subduction zone parameters. We tested correlations with upper plate age, upper plate crustal thickness, subduction velocity, subducting plate dip, and subducting plate age (values taken from *Syracuse et al.* [2010]), which are the parameters controlling slab and/or the mantle wedge's thermal structure (section 1).

The main pressure sensitivity in the thermobarometric calculations is host rock composition, which has a small enough effect that it is not expected to mask primary differences in equilibration pressure. Although it is likely that the composition of the host rock varies between zones, it is clear that irrespective of assumed host composition, the equilibration depths are mostly located within the upper plate.

We find that equilibration pressures have negligible correlation with parameters that control slab thermal structure: slab dip and age, convergence velocity (Figure S3), or the combination of these, the thermal parameter (Figure 5a).

The only parameter with which there is a significant pressure correlation, is upper plate age (Figure 5b). This includes strong positive correlations between the median, mean and range of the equilibration pressures and the upper plate age, of 0.89, 0.91, and 0.91, respectively. We also note that the pressure range increase with upper plate age is mostly due to an increase in the maximum pressures sampled—the minimum pressure is relatively similar between subduction zones, and close to the base of the crust.

It is worth considering if the strong correlation with pressure range could simply be due to the fact that the zones with older upper plate ages have a larger number of samples meeting our filtering criteria. For example Izu is an outlier in terms of number of samples passing our filtering criteria (there are 120, almost double the second largest) and has the largest pressure range. To test this, pressure range is plotted versus the number of samples available, and returns only a moderate correlation (0.57, Figure S2 in Supporting

Information). If Izu is excluded, the correlations remain strong (mean r = 0.87, median r = 0.84, standard deviation r = 0.73, and range r = 0.88). Therefore, the number of samples does not exert a major control on the correlation of upper plate age and equilibration pressure.

We use upper plate age as a proxy for upper plate thickness (as did *Syracuse et al*. [2010]). Although this is reasonable, there are significant uncertainties in oceanic upper plate thicknesses. The values for the upper plate age in *Syracuse et al*. [2010] are chosen as half the age of the oldest part of the plate. By the comparison of age maps and seismic studies [*Müller et al*., 2008; *Wiens et al*., 2006; *Abers et al*., 2014; *Calvert*, 2011], it is clear that the main trends in lithospheric thickness, in particular the order of the youngest, middle ages and oldest upper plates in our data set are probably robust. (a) Upper plate age increases from the Marianas to Izu, as well as from Tonga to Kermadec because the distance from the back-arc spreading center and age of activity increase in those directions. (b) The Antilles upper plate is one of the oldest (Cretaceous), but further affected by subsequent Eocene thinning (Grenada Basin) [*Bouysse*, 1988], so 50 m.y. is probably a reasonable effective age. The Izu upper plate is partly relatively young, but contains large age gradients with maximum ages up to 100 m.y. and may be affected by the collision of the arc with Honshu which also results in a relatively thick crust [e.g., *Calvert*, 2011], so it too is at the high end of overriding plate thickness relative to the other zones we studied. (c) The Marianas upper plate is thicker and colder than Tonga's [*Wiens et al*., 2006], making Marianas and Kermadec the middle range in ages. (d) Scotia has a very young back arc and thin lithosphere [*Wiens et al*., 2006], and the New Britain back arc is similarly young (1–4 Ma) [*Holm et al*., 2016]. Tonga's back arc is also young (most recent spreading from 7 to 0 Ma, older spreading from 35 Ma) [*Sdrolias and Müller*, 2006] and appears to be relatively hot [*Wiens et al*., 2006; *Abers et al*., 2014]. Thus, in spite of the uncertainties in lithospheric thickness, the order of the zones would be unlikely to change significantly, and this is what yields the correlation between the pressure range and upper plate age.

Turner and Langmuir [2015b] inferred from their global data set that lithospheric thickness correlates with crustal thickness. Such a correlation can be understood if both crust and lithosphere are affected by the same tectonic or magmatic thickening or thinning processes [*Turner et al*., 2016; *Karlstrom et al*., 2014]. However, we do not find a correlation of lava thermobarometric pressures with arc crustal thicknesses from either the *Syracuse et al*. [2010] or *Turner and Langmuir* [2015b] compilations (the latter is shown Figure S3). It is worth recognizing that crust and lithospheric thicknesses are also affected by distinct processes (like thermal and convective erosion of the lithosphere). Many of the zones we study, have been subject to multiple episodes of back-arc rifting which cumulatively built the arc crust, but each time renewed much of the upper plate lithosphere. This may well explain why we find no correlation between crust and lithospheric thickness in our data set of intraoceanic subduction zones.

In contrast to the pressure estimates, equilibration temperature estimates are sensitive to primary water content and it is likely that that this varies significantly between and within zones [e.g., *Turner and Langmuir*, 2015b; *Plank et al*., 2013], and hence trends with temperature may become obscured. Indeed, when an assumption of constant water content across all zones is employed, no meaningful trends emerge.

3.2.3. Along-Arc Variations

Systematic variation in equilibration pressure range with upper plate age can be further illustrated by examining the distribution of pressures along individual arcs. Figure 6 shows the variation along the Izu-Southern Marianas and Tonga-Kermadec arc segments. The deepening of maximum pressures can be clearly seen going from the younger upper plate in the southern Marianas to the older/thicker upper plate in Izu along the IBM trench (as shown by gray lines). Similarly, along the Tonga-Kermadec trench, the upper plate age increases southward as do the maximum pressures and the pressure ranges.

Figure 6 also showcases that although the overall trends are clearly distinguished both in averages (Figure 5) and in along-arc sections, there is significant variability from island to island, even between nearby islands, in both maximum pressure and range. For example, at Kao volcano in Tonga, located at −20° south, there are lavas which sample pressures on average 0.7 GPa deeper than those from nearby Tofua volcano, despite being located only 10 km apart.

If we assume that the samples from Kao equilibrated with Mg# 0.9, and the samples from Tofua equilibrated with Mg# 0.92 with all other parameters equal, then the pressures can be reconciled. Although it is not impossible that such short-scale variations in mantle composition exist, sampling bias must also be

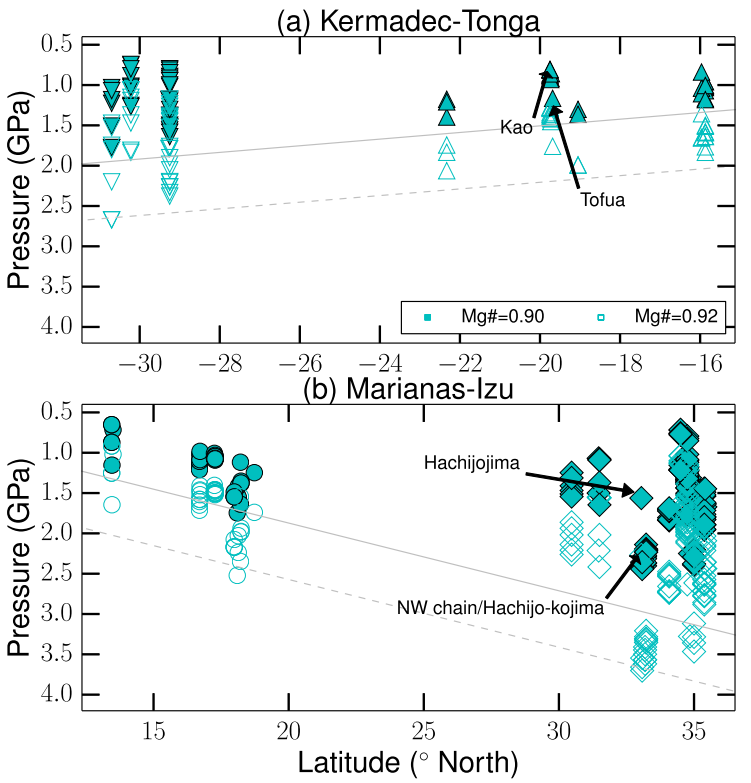

Figure 6. Along-arc pressure variations for the (a) Tonga-Kermadec and (b) Izu-Marianas arcs, calculated assuming 4 wt % H_2O, $Fe^{3+}/Fe_{total} = 0.15$, and at both host Mg# = 0.9 and Mg# = 0.92. Islands labeled are those referred to in text. Gray lines are hand-drawn and illustrate the change in the deepest pressure estimates along the arcs.

considered. The number of samples at most islands is small, usually <20, with some islands only having one or two analyses that meet our filtering criteria. Given the overall large range of equilibration pressures observed, caution needs to be exercised when analyzing results from a single volcano or island.

Similar short-scale variability is also seen in Izu at around 33°N. The pressures here vary by ~1 GPa over 25 km surface distance at a constant host Mg#. One sample in the southern part of this area, from the study of *Taylor and Nesbitt* [1998], is from the island of Hachijojima (which is composed of two volcanoes, Nishiyama and Higashiyama), and records a pressure of 1.5 GPa (at 0.9 host Mg#). The samples with apparently larger equilibration pressures, from the study of *Ishizuka et al.* [2008], were dredged to the north of the island and are submarine samples that are part of a chain extending to the NW of Hachijojima, and also from Hachijo-kojima, a volcano to the west of Hachijojima. They conclude that the samples from the chain to the NW of Hachijojima and Hachijo-kojima are from the same primary magma source as the Hachijojima volcano and are the result of lateral magma transport along arc within the crust. This indicates different depths of equilibration for magmas from the same source. Where there are a large number of samples available at an island, pressures over a range of ~1 GPa can be sampled, reinforcing the notion that short-scale pressure differences may be due to insufficient sample size at a particular location.

3.2.4. Comparison With Turner and Langmuir Data Set

The only statistically significant trend in our analysis is that of equilibration pressure and upper plate age. To further test the robustness of this trend, we apply a similar analysis to the database compiled by *Turner and Langmuir* [2015a], who used somewhat different criteria of sample age and quality in their selection. When compiling their database, *Turner and Langmuir* [2015a] selected samples with the aim to compare lavas that had experienced a similar level of fractionation, e.g., only considering samples with MgO content between 5.5 and 6.5 wt %. Within this range, the amount of fractionation can affect major element concentrations, and therefore the pressure estimated using the *Lee et al.* [2009], as shown in Figure S1. They additionally filtered for Eu anomalies that indicate that samples had been affected by either plagioclase fractionation or mixing with an end-member which has undergone plagioclase fractionation (Eu anomaly <0.85) or plagioclase accumulation (Eu anomaly >1.1). Although, as discussed previously, we expect our calculated P, T to not be significantly affected by potential plagioclase fractionation, this more stringent filtering process could illuminate possible mixing or accumulation of plagioclase. We refiltered the *Turner and Langmuir* [2015a] database for samples with MgO contents between 6 and 10 wt %, and with an Eu anomaly in the range of 0.85–1.1, to enable comparison with our database.

The relationship between pressure and upper plate age for the *Turner and Langmuir* [2015a] database is shown in Figure 7. Similar strong correlations are seen with median and mean pressures and upper plate

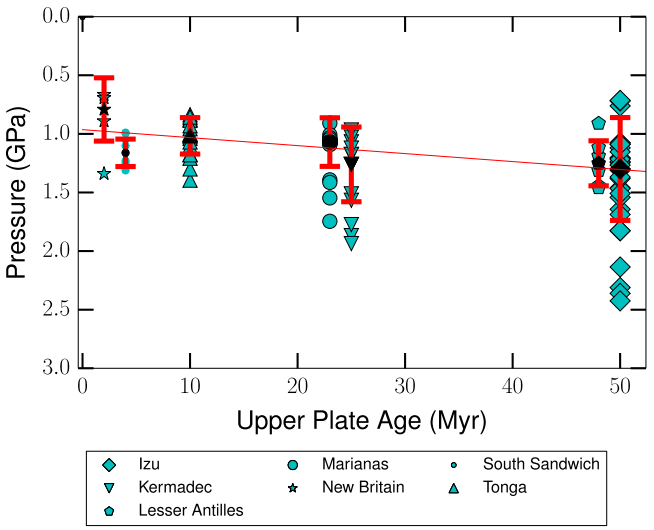

Figure 7. Same as Figure 5, but for the data set of *Turner and Langmuir* [2015a]: pressure estimations for primitive water content of 4 wt % H_2O, host Mg# = 0.9, Fe^{3+}/Fe_{total} = 0.15 versus upper plate age. Each cyan point is an individual sample pressure. Black markers are medians, and red error bars are standard deviations for each arc data set. Note that the Lesser Antilles actually has an upper plate age of 50 Myr, but has been offset slightly to enable clearer viewing of data. This is the same for the Southern Marianas (actual 25 Myr upper plate age) and South Sandwich (actual 2 Myr upper plate age). As with our data set, there is a significant correlation between upper plate age and the pressure distribution, with mean: r = 0.75, median: r =0.73, standard deviation: r = 0.54, range: r = 0.61.

age (0.73 and 0.75, respectively), although the correlation with range is somewhat weaker, at 0.61, as is the correlation with the standard deviation, 0.54. Similar to the analyses with our database, no correlations are found with any other subduction zone parameters (Supporting Information Figure S3).

3.2.5. Comparison With Published Continental P, T

In the future, it would be useful to extend the analysis to continental arcs. A few have already been studied previously. *Kelemen et al.* [2003] compiled P, T estimates from a few active arcs (including data points from Japan and Cascadia), while *Lee et al.* [2009], *Elkins-Tanton et al.* [2001], *Ruscitto et al.* [2010], and *Watt et al.* [2013] compiled more comprehensive data sets for Cascadia and the southern Chile Volcanic Zone, respectively. In all cases, they find pressure estimates that range from about the base of the Moho to 1.5–2.5 GPa. Their temperature estimates are much higher than expected for any continental geotherms and follow a trend that more or less parallels the solidus. Lithospheric thicknesses in continental back-arc regions tend to be around 50–70 km [*Currie and Hyndman*, 2006], with those for Cascadia between 55 and 75 km [*Currie and Hyndman*, 2006], and those for Southern Chile between 60 and 70 km [e.g., *Currie and Hyndman*, 2006; *Hickey-Vargas et al.*, 2016], for distances <100 km from the trench. Thus, the range of thermobarometric pressures overlaps and possibly extends slightly below these lithospheric thicknesses. From this limited set, it appears the available continental data reflect very similar conditions as those we find for our intraoceanic primitive arc lavas.

4. Discussion and Interpretation: Comparison With Numerical Models

It is clear from the analyses above as well as previous work [e.g., *Kelemen et al.*, 2003; *Ruscitto et al.*, 2010; *Weaver et al.*, 2011; *Watt et al.*, 2013], that the prevalence of elevated temperatures coupled to shallow pressures in petrologically determined P, T estimates is not straightforward to reconcile with predictions from thermal models. We next evaluate the extent of disagreement between models and equilibration P, T conditions. Because of the apparent control that upper plate age has on equilibration pressures, we discuss results by using the cases of Tonga and the Lesser Antilles (Figure 8), which have upper plate ages of 10 Myr (young) and 50 Myr (comparatively old), respectively. Models for all other zones are included in Figure S4 of Supporting Information.

For each subduction zone, we evaluate whether the P, T conditions inferred from thermobarometry correspond to numerically predicted conditions in the mantle wedge. We perform comparisons of thermal models and thermobarometry for a range of host Mg# (0.90, 0.91, and 0.92), and primary H_2O contents (0, 4, and 8 wt %). Uncertainties stemming from assumed $Fe^{3+}/\Sigma Fe$ in thermobarometric calculations are used to assign error values of ±0.15 GPa and ±22°C to the petrologic PT conditions for this comparison.

Several studies of wedge models have documented that the main controls on wedge temperature are subduction velocity, slab dip, upper plate thickness, decoupling depth, and mantle temperature [*van Keken et al.*, 2002; *Syracuse et al.*, 2010; *Wada et al.*, 2008; *Conder*, 2005; *England and Wilkins*, 2004; *Le Voci et al.*, 2014; *Karlstrom et al.*, 2014; *Turner et al.*, 2016]. The first two parameters are zone specific and well constrained by data [*Syracuse et al.*, 2010]. Upper plate thickness is also zone specific, but as discussed above

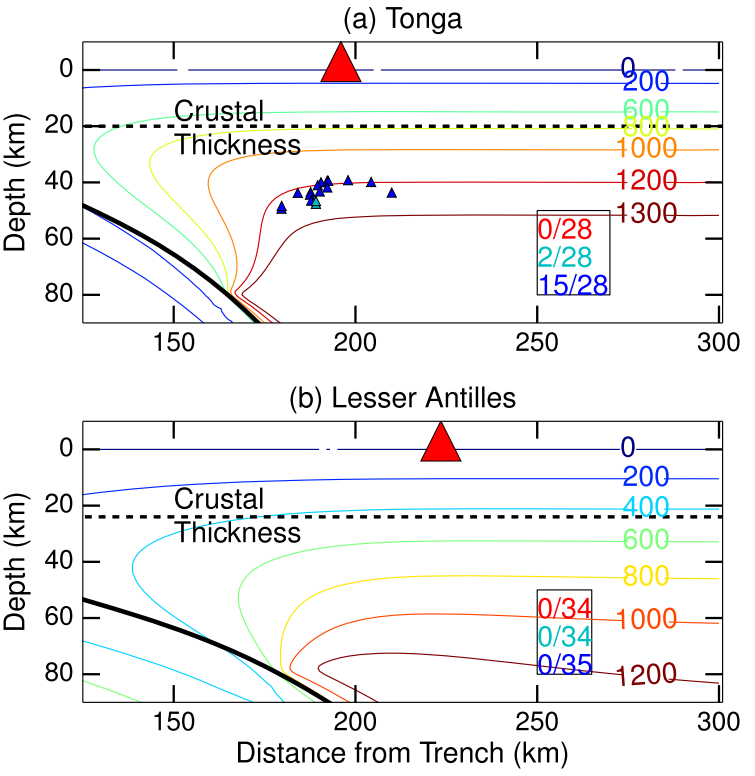

Figure 8. Reference thermal model cases (1350°C potential temperature, 80 km decoupling depth) for Tonga and the Lesser Antilles, and positions of sample P, T at Mg# = 0.9, Fe^{3+}/Fe_{total} = 0.15, and assumed H_2O contents of 0 (red), 4 (green), and 8 wt % (blue), there where samples can be reconciled with model P, T structure within 0.15 GPa and 22°C. The numbers in the black boxes indicate the number of samples that can be reconciled with the model conditions out of the total number of samples, colored by assumed H_2O content. The position of the arc is plotted as a red triangle. Dashed black line marks the crustal thickness below the arc from *Clift and Vannucchi* [2004]. Black lines are the slab surface coordinates, as given in *Syracuse et al.* [2010, Supporting Information]. Only the top-central part of the model domain is shown. In Tonga the upper plate is young enough for about half the samples with 8 wt % H_2O to be plotted, while none of the sample P, T conditions can be found within the Lesser Antilles model.

less well constrained. Furthermore, upper plate thickness may vary due to (a) dynamic interaction with wedge flow and (b) inherited variations in plate thickness. The first process is incorporated in the models and as a result upper plate thickness evolves with time (i.e., until the zone-specific upper plate age is reached). This evolution is strongly affected by the choice of decoupling depth [*Syracuse et al.*, 2010; *Wada et al.*, 2008; *Conder*, 2005]. We start from a simple half-space cooling plate structure and do not consider any inherited thickness variations, which have, for example, been proposed to affect arc migration [*Karlstrom et al.*, 2014]. However, the results will show that the disagreements between model structure and thermobarometric conditions are more fundamental than can be reconciled with inherited thickness variations. We will use the Tonga models to illustrate the effects of decoupling depth and mantle temperature. Comparison with the Antillean case and models for all the other zones clearly highlights the effect of plate thickness.

4.1. Tonga

Tonga has a very young upper plate age of 10 Myr and a rapid subduction velocity of 16.58 cm/yr. Mantle potential temperatures have been inferred to vary from 1350 to 1500°C in back-arc basins [*Kelley et al.*, 2006] and have been proposed to be particularly high in the Lau Basin (1440°C), possibly because of the proximity of the Samoan plume [*Kelley et al.*, 2006; *Nebel and Arculus*, 2015]. We test (1) the reference mantle potential temperature of 1350°C as well as (2) a hotter wedge of 1421°C (the temperature in the models of *Syracuse et al.*, 2010]). In addition, if decoupling is controlled by rheology [*Arcay et al.*, 2005; *Arcay*, 2012], a shallower decoupling depth than the reference value of 80 km may be expected, so as an end-member, we also test (3) a model where thickness of the fixed upper plate and the decoupling depth are set to 10 km. Note that previous studies [*Syracuse et al.*, 2010; *Wada et al.*, 2008] have shown that globally decoupling depth can probably not vary much more than ±5 or 10 km around 80 km depth, so this is indeed an end-member case. A summary of how many sample P, T conditions are reconciled in each model case for Tonga is given in Table 2.

In the reference case (1), most sample P, T can only be reconciled if an extreme case of 8 wt % H_2O and a host 0.92 Mg# residue is assumed (i.e., the combined coolest and deepest possible temperatures and pressures for the sample set). The position of these P, T conditions on this model are shown in Figure 8a. It is important to note that no samples would match thermal model conditions if the models were run for 20

Table 2. Number of Sample P, T That Are Able To Be Reconciled for Each of the Three Model Cases for Tonga, Exploring Uncertainty in Host Mg# and H_2O

Simulation	Host Mg#	0 wt % H_2O	4 wt % H_2O	8 wt % H_2O
(1) Reference	0.9	0/28	2/28	15/28
1350°C	0.92	0/28	6/28	28/28
(2) Hotter	0.9	0/28	8/28	28/28
1421°C	0.92	0/28	28/28	28/28
(3) 10 km	0.9	0/28	27/28	28/28
decoupling	0.92	2/28	28/28	28/28

Myr to a quasi steady state [*Kelemen et al*., 2003; *Syracuse et al*., 2010]. H_2O concentrations of 8 wt % are high compared with melt inclusion measurements from samples worldwide, and within Tonga specifically, where they vary from 2.9 to 4.9 wt % (six samples) [*Plank et al*., 2013].

The 1421°C model case (2) is able to reconcile more sample P, T with model mantle temperatures at 4 wt % H_2O, closer to measured melt inclusion values, although a heavily depleted host (Mg# = 0.92) is still required. If a constant H_2O content is assumed, the temperature estimates of the samples fall within a relatively small temperature range and over a relatively large pressure range. These conditions are met at the point where the isotherms are close to vertical, at the boundary of the cold nose of the wedge. We note that this lies approximately below the arc for a decoupling depth of 80 km.

To test the suggestion made by *Kelemen et al*. [2003] that erosion of the upper plate above the wedge corner can account for the discrepancy between models and petrologic mantle *P*, *T* estimates from lavas, we examine a model where we set the decoupling depth to 10 km, case (3). Such a shallow decoupling depth is indeed able to reconcile a significant number of sample P, T points, at both 4 and 8 wt % H_2O. However, (i) this configuration allows wedge flow to erode into the overlying lithosphere close to the trench and (ii) the positions where sample *P*, *T* estimates can be reconciled are located 30–60 km trenchward from the arc, thus requiring a mechanism that would transport the magmas laterally before rising below the arc. Elevated temperatures beneath the fore arc, as predicted in this model, are inconsistent with observations of low heat flow and low seismic attenuation, in addition to pervasive seismic indications of serpentinization and the occasional occurrence of seismicity, which indicate that the fore-arc mantle is cold [*Bostock et al*., 2002; *Rychert et al*., 2008; *Wada and Wang*, 2009]. Although *Kelemen et al*. [2003] matched across-arc heat flow gradients with their models, they aligned models at the maximum heat flow, without using observed subduction zone geometries as a constraint. Our models, which utilize the subduction geometries of *Syracuse et al*. [2010], highlight the spatial discrepancy between maximum upper plate thinning and arc positions in cases with a shallow decoupling depth, which lead to substantial upper plate thinning directly above the wedge corner.

In summary, if the Tonga wedge has elevated temperatures, and/or the upper plate is at the thin end of the range expected for this zone, then the sample P, T conditions may reflect mantle wedge conditions. The position of the magmatic equilibration conditions places them on the transition into the "cold nose" of the mantle wedge, where isotherms are near vertical.

The predominantly shallow and hot pressure and temperature conditions we determine may represent reequilibration conditions, perhaps at a rheological boundary near the base of the lithosphere and at the transition from fore-arc corner to the wedge. If on the other hand, the conditions at Tonga reflect the location of primary melt generation, it would imply that the main melting conditions are only reached at depths right below the upper plate.

4.2. Lesser Antilles

In contrast to Tonga, the Lesser Antilles has a relatively old (50 Myr) and, hence, thick upper plate, with subduction occurring at ~1.75 cm/yr [*Syracuse et al*., 2010]. Figure 8b shows the thermal structure for the reference case of the Lesser Antilles. The thick overriding lithosphere dictates that no sample P, T can be reconciled with the thermal model, regardless of assumed H_2O content or host Mg#. There is no reason to assume the mantle would be exceptionally hot, but even extremely high (>1500°C) temperatures would not sufficiently thin the lithosphere and reconcile the petrologic sample P, T with the modeled structure. Only in the 10 km decoupling case, can some P, T conditions be reconciled with our model. However, similar

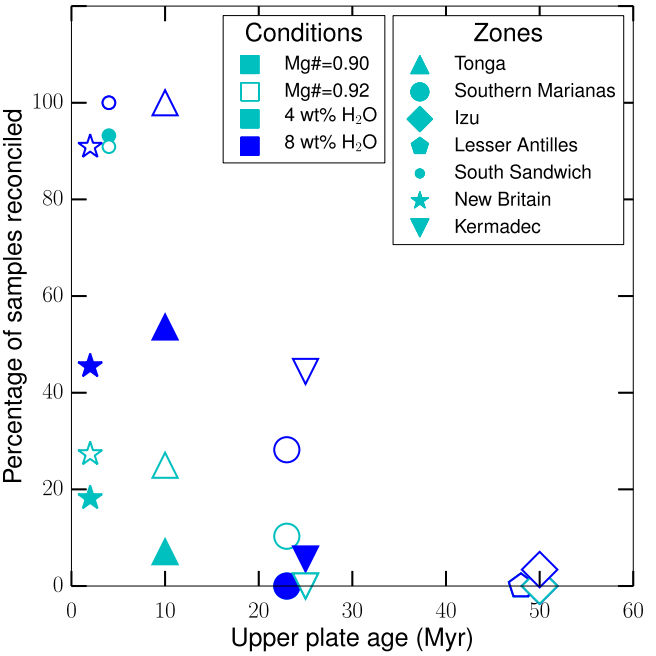

Figure 9. Summary of percentage of samples from each subduction zone that are able to be reconciled with their respective model thermal outputs. Full symbols are for an assumed host Mg# of 0.9, hollow symbols for 0.92. Cyan indicates an assumed primary H_2O content of 4 wt %, blue is 8 wt %. In many cases no samples can be reconciled irrespective of assumed conditions, and so symbols plot at the same point on the *x* axis. In this case the symbol corresponding to the H_2O and Mg# which results in the P, T closest to the model temperatures is the one that is shown.

to Tonga, this case has problems with the position of the P, T points relative to the position of the arc, and comparison with heat flow and seismic attenuation data. A model snapshot at an earlier time of 20 Myr is also unable to reconcile any P, T points.

Hence for the Antillean case, it is clear that the sample P, T conditions do not represent the original source melt conditions, and must correspond to a reequilibration at lithospheric depths. However, this reequilibration process does need to involve significant heating of the lithosphere to be reconciled with the high temperature estimates from thermobarometry.

4.3. All Zones

Considering all of our chosen subduction zones (Figure 4), results fall between the two end-member cases of Tonga and the Antilles (Figure 8). Figure 9 summarizes the findings, illustrating the percentage of the P, T points for each zone that can be reconciled with modeled thermal structure for host Mg# 0.9 and 0.92 and water content of 4 and 8 wt %. For very young upper plates, most of the samples could plausibly represent primary mantle wedge conditions. However, the number of samples that can be reconciled decreases rapidly with increasing upper plate age and thickness, and is only about half for a 10 Myr upper plate like Tonga and zero for upper plates older than 20 Myr.

An intriguing aspect of the data is that thermobarometric conditions always require a near vertical isotherm (e.g., Figure 8), which is only found at the edge of the cold nose. While in the youngest upper-plate cases, P, T conditions may be reconcilable with such a position in the wedge at the edge of the cold nose, for older plates localized thermal erosion below the arc is required to produce such steep isotherms over a wide range of pressures. Note that preexisting lithospheric thickness variations may also induce some steep gradients, but only over a limited depth range, and not necessarily involving thinning below the arc. Thus, our data suggests that lavas last reequilibrate near the base of, or inside, the mantle lithosphere, at strong gradients in viscosity.

4.4. Comparison With Melt-Inclusion P-T Conditions for Marianas

Overall, thermobarometric pressures indicate that lavas equilibrate within the lithosphere, i.e., much shallower than most suggestions of magma-generation depth (Figure 1). In contrast to the whole-rock compositions we used, melt inclusions may capture more primitive melts. Indeed, such melt-inclusion data have been interpreted to represent original melting conditions at high pressure [*Schiano*, 2003; *Le Voyer et al*., 2010; *Kelley et al*., 2010]. We compare in Figure 10 our samples from the Marianas, with the melt inclusion data for this arc of *Kelley et al*. [2010], who also used the *Lee et al*. [2009] thermobarometer to analyze the equilibration conditions using data on water content from the same melt inclusions.

The equilibration pressures of the melt inclusions of the *Kelley et al*. [2010] data set (which includes samples from *Shaw et al*. [2008]) significantly overlap with the pressures of the data set presented here, with the exception of Guguan, where melt inclusion derived pressures are ~0.5 GPa deeper than the whole-rock samples of the data set of this study. And indeed, both data sets span a wide range of pressures, together ranging from slightly less than 1–2.6 GPa.

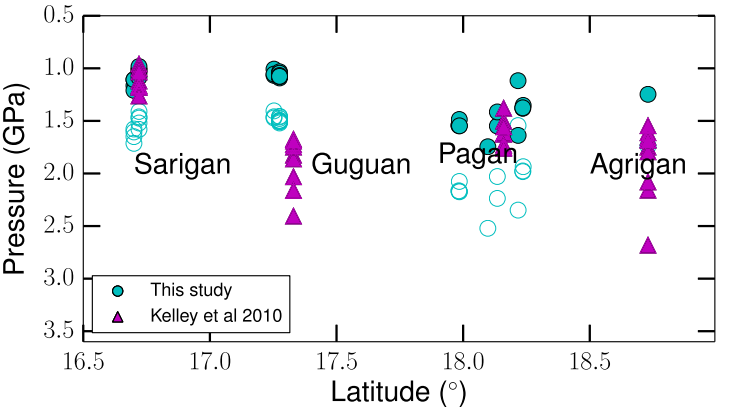

Figure 10. Comparison of the latitudinal variation in equilibration pressures inferred for the Southern Marianas for our data set with the melt inclusion data of *Kelley et al.* [2010]. The equilibration P, T of the samples from our database are estimated at both 0.9 and 0.92 Mg#. The melt-inclusion P show are those calculated by *Kelley et al.* [2010] in their paper, assuming host Mg# = 0.9.

If we plot the P, T conditions of the *Kelley et al.* [2010] melt inclusions on the Marianas thermal structure (Figure 11), more of the melt inclusion pressures and temperatures can be reconciled with the model conditions, but still only about 2/3 of the samples match, even when assuming a high primary water content (8 wt %). If we assume an original water content of 8 wt %, these points plot at the base of the thermal lithosphere, i.e., barely in the mantle wedge. Only one to three of the largest pressures out of the total of 35 points correspond to depths that may fall below the upper plate thermal boundary layer. Interestingly, most of the points in *Kelley et al.* [2010] follow a solidus-parallel trend, except a few of the deepest points which form a somewhat steeper, more adiabat-like trend, as would be compatible with a mantle provenance. Thus, it appears that only a few of the melt inclusions record primary melt conditions in the mantle wedge, while most of them reflect, as do the whole-rock data, reequilibration during melt ascent through the lithosphere.

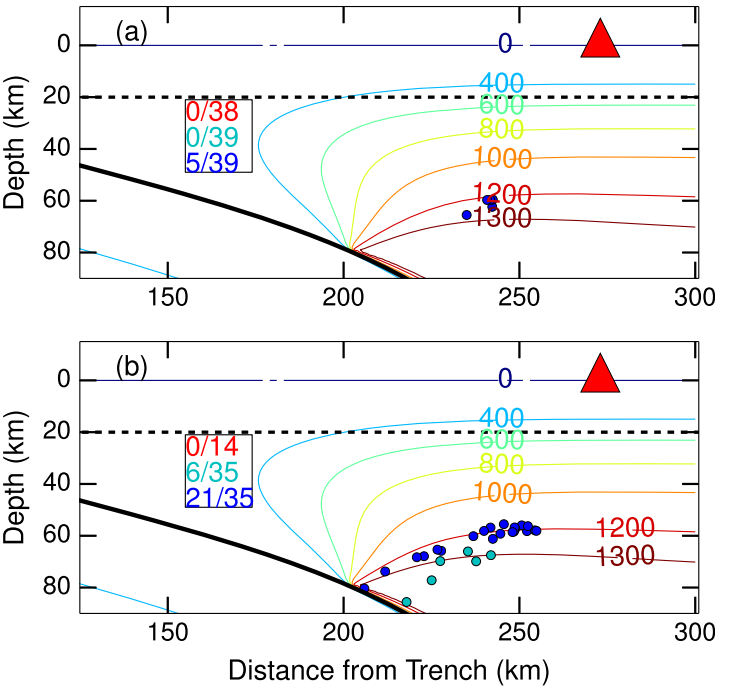

Figure 11. Comparison of Southern Marianas sample P, T with thermal model conditions (1350°C, 80 km decoupling depth), for our (a) sample set and (b) the melt inclusion data set of *Kelley et al.* [2010]. Format of the figure is the same as Figure 8. We calculated P, T for both data sets using host Mg# = 0.9, Fe^{3+}/Fe_{total} = 0.15, and assumed H_2O contents of 0 (red), 4 (green), and 8 wt % (blue). Figure format as in Figure 8, and as in that figure only the part of the model domain around the wedge corner is shown. The numbers in the black boxes indicate the number of samples that can be reconciled with the model conditions out of the total number of samples, colored by assumed H_2O content. Even for the melt inclusion data, few samples plot within the convecting wedge.

4.5. Localized Thermal Erosion of the Upper Plate

It is clear that when models are run to steady state or the upper plate is older than 20 Myr, thermobarometric P, T conditions cannot be easily reconciled with our current models of the mantle wedge's thermal structure. In such cases, a mechanism for locally eroding the lithosphere is required, such that hotter material can be advected to shallower depths. As emphasized above, removing or substantially shallowing the decoupling depth is inconsistent with observations such as fore-arc heat flow and seismic structure of the wedge corner [*Kincaid and Sacks*, 1997; *Hyndman and Peacock*, 2003; *Currie and Hyndman*, 2006; *Rychert et al.*, 2008]. Small-scale convection, which is suppressed at the viscosities examined herein, is able to thin the overriding lithosphere by up to 10 km [*Wirth and Korenaga*, 2012; *Le Voci et al.*, 2014; *Davies et al.*, 2016], but this is insufficient to

reconcile our P, T estimates, similarly to preexisting variations in lithospheric thickness [e.g., *Karlstrom et al*., 2014], which may span a somewhat larger depth range, but still not the whole depth of the lithosphere from the Moho downward.

Alternatively, it has been suggested that the P, T conditions recorded by the lavas may represent transient conditions of migrating melts, rather than lithospheric temperatures, with the main argument for transient conditions being that such high Moho temperatures would result in extensive melting of the lower crust for which there is no evidence [e.g., *Elkins-Tanton et al*., 2001; *Ruscitto et al*., 2010]. However, *Kelemen et al*. [2003] refutes this argument and prefers a lower crustal composition that would not melt at Moho temperatures of 1200–1400°C. Furthermore, the P, T trends delineated by the data are not like the melt adiabats expected for migrating melts. Nonetheless, could it be conceivable that the high T are reflecting a process by which magmas were generated at these temperatures and, after reaching a shallow depth, do not thermally equilibrate with the surroundings? This notion is problematic, as it is inconsistent with the basic premise of the thermobarometer, which assumes chemical reequilibration of SiO_2 [*Lee et al*., 2009]. Silicon has a very low diffusion coefficient in basaltic magma (10^{-10} m^2/s in wet basaltic melts [*Zhang et al*., 2010]), about 4 orders of magnitude lower than thermal diffusivity (10^{-6} m^2/s [*Turcotte and Schubert*, 2014]), and so if SiO_2 is able to chemically equilibrate, then the magmas must be in thermal equilibrium. If on the other hand, the magmas were not fully chemically reequilibrated, then the recorded P, T conditions would be an overestimate of the pressures, further increasing the discrepancy between thermal model and magma P, T conditions. In this case, temperatures could also be an overestimate, however, the fact that magmas must, in part, have reequilibrated as they record lithospheric P conditions, indicates that the much more rapid thermal reequilibration was likely complete and hence high temperatures at lithospheric depths would still be required.

Hence, localized thermal modification of the lithosphere appears to be necessary to reconcile models and thermobarometric P, T conditions. As suggested by *Weaver et al*. [2011], the thermal erosion process proposed by *England and Katz* [2010] provides a viable mechanism. In this process, melts with water contents ranging from "anhydrous" (in *England and Katz* [2010] this refers to a mantle water content of 200–500 ppm) to water saturated are generated. Melts generated within the anhydrous melting region, a relatively small region located within the corner of the wedge, follow the anhydrous solidi upward until they reach the location of the shallowest anhydrous solidi. Once this point is reached, the melts heat the mantle/lithosphere above, deflecting all solidi from anhydrous to wet upward. All melts subsequently produced follow their respective solidi up to this thermally eroded part of the mantle, and then up through the lithosphere to form the arc. According to their model, the amount that the isotherms are deflected upward depends on the ratio of heat transfer by the melt (i.e., melt flux) and conductive loss of heat through the lithosphere [*England and Katz*, 2010].

We apply the thermal erosion model of *England and Katz* [2010] to our thermal structures. Derivation of equations that describe the process can be found in *England and Katz* [2010, Supporting Information]. We use the same input constants, except that we double the magma production rate to 8×10^{-3} kg m^{-1}, which *England and Katz* [2010] acknowledge may be a more realistic value. We choose the 1300°C isotherm as the hottest one to be advected (rather than the 1200°C one used in *England and Katz* [2010]) to allow erosion to affect the whole thermal boundary layer of our models. We assume that the region of melt advection is 15 km wide and positioned directly below the arc, which is more or less there where the unperturbed isotherms reach their shallowest depth, consistent with *England and Katz*'s [2010] hypothesis that this point (which corresponds to where the temperature approach the anhydrous solidus most closely) controls the location of the arc. Applying this to the reference model of the Lesser Antilles now allows 94% of the P, T points to be reconciled, at Mg# = 0.9 and 8 wt % H_2O, and 88% of the 36 points for Mg# = 0.9 and 4 wt % H_2O (Figure 12), suggesting that this is indeed a viable mechanism.

A further advantage of a localized thermal erosion model is that it produces strong lateral strength gradients in the lithosphere over a broad range of depths. This provides a logical explanation for why we find pressures corresponding to broad depth ranges, and depth ranges that correlate with overriding plate age, i.e., thickness. Note that the data P, T trends are also consistent with such a local thermal erosion mechanism, as it will allow adiabatic melting to proceed upward over the whole depth range where the lithosphere has been replaced by asthenospheric temperatures.

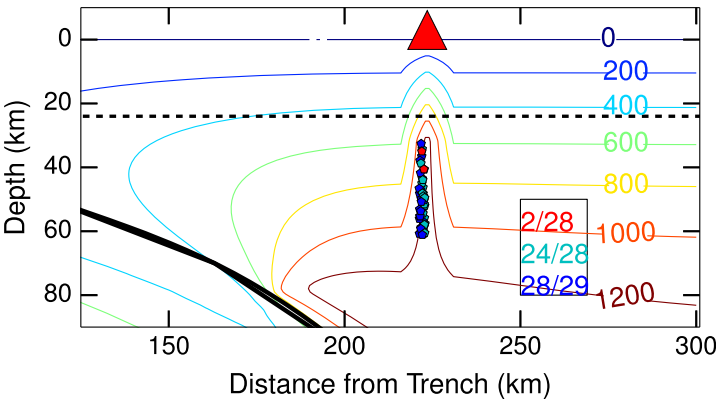

Figure 12. Comparison of sample P, T with numerical model outputs (1350°C, 80 km decoupling depth) for the Lesser Antilles after the application of the thermal erosion process of *England and Katz* [2010]. Format of the figure is the same as Figure 8. P, T estimates are for host Mg# = 0.9, $Fe^{3+}/Fe_{total} = 0.15$, and assumed H_2O contents of 0 (red), 4 (green), and 8 wt % (blue). The numbers in the black boxes indicate the number of samples that can be reconciled with the model conditions out of the total number of samples, colored by assumed H_2O content. Pentagons are plotted where a sample P, T can be found in the model. Now the majority of samples at a water content of 8 wt % can be reconciled.

4.6. Further Consequences of Thermal Erosion

Local thermal modification of the lithosphere is consistent with seismic images documenting localized low velocity and high attenuation (low-Q) zones below several arcs that span the depth range of the lithosphere [*Zhao et al*., 1994, 1997; *Rychert et al*., 2008]. Such signatures have commonly been attributed to the presence of melt. However, bringing material of mantle temperatures to such shallow depths is also an efficient way of lowering seismic velocities, due to the increasing contribution of anelasticity with decreasing depth [e.g., *Goes et al*., 2012]. Hence, our results indicate that the seismic signature may well be a combination of high temperatures and the presence of melt. Furthermore, the seismic signatures agree with a localized thermal effect rather than a larger-scale upper plate thinning above the wedge corner, as was previously proposed by *Kelemen et al*. [2003].

Field observations of exhumed arcs are also consistent with the subarc mantle lithosphere being pervasively heated by intruded melts up to the base of the crust (see compilation and data by *Kelemen et al*. [2003] for the Talkeetna, Alaska, and Kohistan, Pakistan exhumed arcs).

Finally, local thermal erosion of the lithosphere would also be expected to lead to lithospheric weakening. Formation of a localized zone of weakness below the arc is consistent with the observation that back-arc spreading often splits the previous arc, e.g., in Tonga and Marianas [*Karig*, 1970, 1971]. This same process of melt-related weakening has also been invoked to aid continental rifting, based on geophysical and surface observations of the process in Afar [*Ebinger and Casey*, 2001; *Buck*, 2006].

5. Conclusions

We present a study of equilibration pressures and temperatures of intraoceanic subduction zone lavas and compare these conditions with those predicted by kinematically driven models of the wedge's flow regime and thermal structure with geometries from *Syracuse et al*. [2010] for each subduction zone. We draw the following conclusions:

1. Consistent with a number of previous studies of thermobarometric equilibration conditions of mantle melts [*Elkins-Tanton et al*., 2001; *Kelemen et al*., 2003; *Lee et al*., 2009; *Weaver et al*., 2011] we find that for all intraoceanic arcs in our compilation, equilibration temperatures are relatively high (averaging ~1300°C) and pressures are relatively shallow (averaging ~1.1 GPa).
2. We find that pressures span a large range in each arc, more or less comprising the full depth of the upper plate from the Moho to the thermal base of the lithosphere.
3. There are positive correlations of the mean, median, and range of equilibration pressures within each arc with the age of the upper plate, consistent with an upper plate thickness control on the petrologic P, T conditions.
4. The temperature conditions likely equate to lithospheric temperatures where the samples reequilibrated, as the thermobarometer requires chemical equilibration, which is many orders of magnitude slower than thermal reequilibration, making it highly unlikely that these represent transient thermal conditions.
5. Pressures and temperatures can only be reconciled with wedge thermal models if the upper plate is thin (equivalent to an age of <10 Myr). Models with older upper plates (thicker lithospheres) are inconsistent with sample pressures and temperatures.

6. A thermal erosion process, by which melts locally erode the lithosphere below the arc, as previously suggested by *England and Katz* [2010] to explain the focusing of volcanism along a linear arc, once applied to the models, is able to reconcile the predicted thermal structure with the equilibration pressures and temperatures inferred from the lavas. Such local weakening explains the wide range of equilibration pressures all corresponding to high temperatures.

A consequence of the reequilibration process, which appears to be continuous from the mantle wedge throughout the rise through the lithosphere, is that the lithosphere is locally warmed and weakened below the arc. In this process, the geotherms follow an adiabatic melting trend and the apparent melt fractions stay relatively constant in the range 10–20%. There are potential implications of this reequilibration process. The chemical composition of the melts may be altered, and, as such, affect the interpretations of subduction zone geochemistry. Trace element ratios are likely unaffected, as reequilibration with mineral assemblages that are similar to the mineral assemblages from which the magma first formed will have little effect on the ratios, however absolute major, minor and trace element concentrations may be affected. The lack of correlation of the reequilibration pressures with other subduction parameters, such as thermal parameter, does not preclude the possibility that these parameters could have a control on where these magmas are first generated, but information on this process would be lost in the reequilibration process.

Acknowledgments
We thank Pierre Bouilhol, Stéphane Rondenay, and John Armitage for discussions and the Applied Modelling and Computation Group for support with Fluidity. We much appreciate the thoughtful and detailed reviews by Leif Karlstrom and Stephen Turner. A.P. was funded by a Janet Watson fellowship from the department of Earth Science and Engineering, Imperial College London, SG by the VoiLA project (NERC grant NE/K010743/1), D.R.D. and C.W. by NERC grant NE/I024429/1, C.W. by NSF OCE-1358091, and D.R.D. by an ARC Future Fellowship (FT140101262).

References

Abers, G., K. Fischer, G. Hirth, D. Wiens, T. Plank, B. Holtzman, C. McCarthy, and E. Gazel (2014), Reconciling mantle attenuation-temperature relationships from seismology, petrology, and laboratory measurements, *Geochem. Geophys. Geosyst.*, *15*, 3521–3542, doi:10.1002/2014GC005444.

Arcay, D. (2012), Dynamics of interplate domain in subduction zones: Influence of rheological parameters and subducting plate age, *Solid Earth*, *3*(2), 467–488.

Arcay, D., M. P. Doin, and E. Tric (2005), Numerical simulations of subduction zones: Effect of slab dehydration on *the mantle wedge dynamics, Phys. Earth Planet. Inter.*, *149*, 133–153, doi:10.1016/j.pepi.2004.08.020.

Behn, M. D., P. B. Kelemen, G. Hirth, B. R. Hacker, and H.-J. Massonne (2011), Diapirs as the source of the sediment signature in arc lavas, *Nat. Geosci.*, *4*(9), 641–646.

Billen, M. I., and M. Gurnis (2001), A low viscosity wedge in subduction zones, *Earth Planet. Sci. Lett.*, *193*(1–2), 227–236, doi:10.1016/S0012-821X(01)00482-4.

Bostock, M., R. Hyndman, S. Rondenay, and S. Peacock (2002), An inverted continental Moho and serpentinization of the forearc mantle, *Nature*, *417*(6888), 536–538.

Bouysse, P. (1988), Opening of the Grenada back-arc basin and evolution of the Caribbean plate during the mesozoic and early paleogene, *Tectonophysics*, *149*, 121–143, doi:10.1016/0040-1951(88)90122-9.

Bremond d'Ars, J., C. Jaupart, and R. S. J. Sparks (1995), Distribution of volcanoes in active margins, *J. Geophys. Res.*, *100*(B10), 20,421–20,432.

Buck, W. (2006), The role of magma in the development of the Afro-Arabian rift system, *Geol. Soc. Spec Publ.*, *259*(1), 43–54.

Cagnioncle, A.-M., E. Parmentier, and L. T. Elkins-Tanton (2007), Effect of solid flow above a subducting slab on water distribution and melting at convergent plate boundaries, *J. Geophys. Res.*, *112*, B09402, doi:10.1029/2007JB004934.

Calvert, A. J. (2011), The seismic structure of island arc crust, in *Arc-Continent Collision, Front. Earth Sci.*, pp. 87–119, Springer-Verlag, Berlin.

Clift, P., and P. Vannucchi (2004), Controls on tectonic accretion versus erosion in subduction zones: Implications for the origin and recycling of the continental crust, *Rev. Geophys.*, *42*, RG2001, doi:10.1029/2003RG000127.

Conder, J. A. (2005), A case for hot slab surface temperatures in numerical viscous flow models of subduction zones with an improved fault zone parameterization, *Phys. Earth Planet. Inter.*, *149*(1), 155–164.

Cooper, L. B., D. M. Ruscitto, T. Plank, P. J. Wallace, E. M. Syracuse, and C. E. Manning (2012), Global variations in H_2O/Ce: 1. Slab surface temperatures beneath volcanic arcs, *Geochem. Geophys. Geosyst.*, *13*, Q03024, doi:10.1029/2011GC003902.

Courtier, A. M., et al. (2007), Correlation of seismic and petrologic thermometers suggests deep thermal anomalies beneath hotspots, *Earth Planet. Sci. Lett.*, *264*(1), 308–316.

Currie, C. A., and R. D. Hyndman (2006), The thermal structure of subduction zone back arcs, *J. Geophys. Res.*, *111*, B08404, doi:10.1029/2005JB004024.

Davies, D. R., C. R. Wilson, and S. C. Kramer (2011), Fluidity: A fully unstructured anisotropic adaptive mesh computational modeling framework for geodynamics, *Geochem. Geophys. Geosyst.*, *12*, Q06001, doi:10.1029/2011GC003551.

Davies, D. R., G. Le Voci, S. Goes, S. Kramer, and C. Wilson (2016), The mantle wedge's transient 3-D flow regime and thermal structure, *Geochem. Geophys. Geosyst.*, *17*, 78–100, doi:10.1002/2015GC006125.

Dumoulin, C., M.-P. Doin, and L. Fleitout (2001), Numerical simulations of the cooling of an oceanic lithosphere above a convective mantle, *Phys. Earth Planet. Inter.*, *125*(1), 45–64.

Ebinger, C., and M. Casey (2001), Continental breakup in magmatic provinces: An Ethiopian example, *Geology*, *29*(6), 527–530.

Elkins-Tanton, L. T., T. L. Grove, and J. Donnelly-Nolan (2001), Hot, shallow mantle melting under the cascades volcanic arc, *Geology*, *29*(7), 631–634.

England, P., and C. Wilkins (2004), A simple analytical approximation to the temperature structure in subduction zones, *Geophys. J. Int.*, *159*(3), 1138–1154.

England, P. C., and R. F. Katz (2010), Melting above the anhydrous solidus controls the location of volcanic arcs, *Nature*, *467*(7316), 700–703.

Gaetani, G. A., T. L. Grove, and W. B. Bryan (1993), The influence of water on the petrogenesis of subduction-related igneous rocks, *Nature*, *365*(6444), 332–334.

Gerya, T. V., and D. A. Yuen (2003), Rayleigh-Taylor instabilities from hydration and melting propel "cold plumes" at subduction zones, *Earth Planet. Sci. Lett.*, *212*, 47–62, doi:10.1016/S0012-821X(03)00265-6.
Gill, J. (2012), *Orogenic Andesites and Plate Tectonics*, vol. 16, Springer, Berlin.
Goes, S., J. Armitage, N. Harmon, H. Smith, and R. Huismans (2012), Low seismic velocities below mid-ocean ridges: Attenuation versus melt retention, *J. Geophys. Res.*, *117*, B12403, doi:10.1029/2012JB009637.
Grove, T., S. Parman, S. Bowring, R. Price, and M. Baker (2002), The role of an H_2O-rich fluid component in the generation of primitive basaltic andesites and andesites from the Mt. Shasta region, N California, *Contrib. Mineral. Petrol.*, *142*(4), 375–396.
Grove, T. L., C. B. Till, E. Lev, N. Chatterjee, and E. Medard (2009), Kinematic variables and water transport control the formation and location of arc volcanoes, *Nature*, *459*, 694–697, doi:10.1038/nature08044.
Grove, T. L., C. B. Till, and M. J. Krawczynski (2012), The role of H_2O in subduction zone magmatism, *Annu. Rev. Earth Planet. Sci.*, *40*, 413–439.
Hall, P. S., and C. Kincaid (2001), Diapiric flow at subduction zones: A recipe for rapid transport, *Science*, *292*(5526), 2472–2475.
Hermann, J., and C. J. Spandler (2007), Sediment melts at sub-arc depths: An experimental study, *J. Petrol.*, *49*(4), 717–740, doi:10.1093/petrology/egm073.
Hickey-Vargas, R., S. Holbik, D. Tormey, F. A. Frey, and H. M. Roa (2016), Basaltic rocks from the Andean Southern Volcanic Zone: Insights from the comparison of along-strike and small-scale geochemical variations and their sources, *Lithos*, *258–259*, 115–132, doi:10.1016/j.lithos.2016.04.014.
Holm, R. J., G. Rosenbaum, and S. W. Richards (2016), Post 8 ma reconstruction of Papua New Guinea and Solomon Islands: Microplate tectonics in a convergent plate boundary setting, *Earth Sci. Rev.*, *156*, 66–81, doi:10.1016/j.earscirev.2016.03.005.
Huene, R., and D. W. Scholl (1991), Observations at convergent margins concerning sediment subduction, subduction erosion, and the growth of continental crust, *Rev. Geophys.*, *29*(3), 279–316.
Hyndman, R. D., and S. M. Peacock (2003), Serpentinization of the forearc mantle, *Earth Planet. Sci. Lett.*, *212*(34), 417–432, doi:10.1016/S0012-821X(03)00263-2.
Ishizuka, O., N. Geshi, J. Itoh, Y. Kawanabe, and T. TuZino (2008), The magmatic plumbing of the submarine Hachijo NW volcanic chain, Hachijojima, Japan: Long-distance magma transport?, *J. Geophys. Res.*, *113*, B08S08, doi:10.1029/2007JB005325.
Karig, D. E. (1970), Ridges and basins of the Tonga-Kermadec island arc system, *J. Geophys. Res.*, *75*(2), 239–254.
Karig, D. E. (1971), Origin and development of marginal basins in the western pacific, *J. Geophys. Res.*, *76*(11), 2542–2561.
Karlstrom, L., C.-T. A. Lee, and M. Manga (2014), The role of magmatically driven lithospheric thickening on arc front migration, *Geochem. Geophys. Geosyst.*, *15*, 2655–2675, doi:10.1002/2014GC005355.
Katz, R. F., M. Spiegelman, and C. H. Langmuir (2003), A new parameterization of hydrous mantle melting, *Geochem. Geophys. Geosyst.*, *4*(9), 1073, doi:10.1029/2002GC000433.
Kelemen, P. B., J. L. Rilling, E. Parmentier, L. Mehl, and B. R. Hacker (2003), Thermal structure due to solid-state flow in the mantle wedge beneath arcs, in *Inside the Subduction Factory*, pp. 293–311, AGU, Washington, D. C.
Kelley, K. A., and E. Cottrell (2009), Water and the oxidation state of subduction zone magmas, *Science*, *325*(5940), 605–607.
Kelley, K. A., T. Plank, T. L. Grove, E. M. Stolper, S. Newman, and E. Hauri (2006), Mantle melting as a function of water content beneath back-arc basins, *J. Geophys. Res.*, *111*, B09208, doi:10.1029/2005JB003732.
Kelley, K. A., T. Plank, S. Newman, E. M. Stolper, T. L. Grove, S. Parman, and E. H. Hauri (2010), Mantle melting as a function of water content beneath the Mariana Arc, *J. Petrol.*, *51*(8), 1711–1738.
Kimura, J.-I., and T. Yoshida (2006), Contributions of slab fluid, mantle wedge and crust to the origin of quaternary lavas in the NE Japan arc, *J. Petrol.*, *47*(11), 2185–2232.
Kincaid, C., and I. S. Sacks (1997), Thermal and dynamical evolution of the upper mantle in subduction zones, *J. Geophys. Res.*, *102*(B6), 12,295–12,315.
Klimm, K., J. D. Blundy, and T. H. Green (2008), Trace element partitioning and accessory phase saturation during H_2O-saturated melting of basalt with implications for subduction zone chemical fluxes, *J. Petrol.*, *49*(3), 523–553.
Konter, J. G., and T. W. Becker (2012), Shallow lithospheric contribution to mantle plumes revealed by integrating seismic and geochemical data, *Geochem. Geophys. Geosyst.*, *13*, Q02004, doi:10.1029/2011GC003923.
Kramer, S. C., C. R. Wilson, and D. R. Davies (2012), An implicit free surface algorithm for geodynamical simulations, *Phys. Earth Planet. Inter.*, *194*, 25–37.
Le Voci, G., D. R. Davies, S. Goes, S. C. Kramer, and C. R. Wilson (2014), A systematic 2-D investigation into the mantle wedge's transient flow regime and thermal structure: Complexities arising from a hydrated rheology and thermal buoyancy, *Geochem. Geophys. Geosyst.*, *15*, 28–51, doi:10.1002/2013GC005022.
Le Voyer, M., E. Rose-Koga, N. Shimizu, T. Grove, and P. Schiano (2010), Two contrasting H_2O-rich components in primary melt inclusions from Mount Shasta, *J. Petrol.*, *51*(7), 1571–1595.
Lee, C.-T. A., W. P. Leeman, D. Canil, and Z.-X. A. Li (2005), Similar V/Sc systematics in MORB and arc basalts: Implications for the oxygen fugacities of their mantle source regions, *J. Petrol.*, *46*(11), 2313–2336.
Lee, C.-T. A., P. Luffi, T. Plank, H. Dalton, and W. P. Leeman (2009), Constraints on the depths and temperatures of basaltic magma generation on earth and other terrestrial planets using new thermobarometers for mafic magmas, *Earth Planet. Sci. Lett.*, *279*(1), 20–33.
Lee, C.-T. A., P. Luffi, V. Le Roux, R. Dasgupta, F. Albaréde, and W. P. Leeman (2010), The redox state of arc mantle using Zn/Fe systematics, *Nature*, *468*(7324), 681–685.
Lytle, M. L., K. A. Kelley, E. H. Hauri, J. B. Gill, D. Papia, and R. J. Arculus (2012), Tracing mantle sources and Samoan influence in the northwestern Lau back-arc basin, *Geochem. Geophys. Geosyst.*, *13*, Q10019, doi:10.1029/2012GC004233.
Marschall, H. R., and J. C. Schumacher (2012), Arc magmas sourced from mélange diapirs in subduction zones, *Nat. Geosci.*, *5*(12), 862–867, doi:10.1038/ngeo1634.
McCulloch, M. T., and J. Gamble (1991), Geochemical and geodynamical constraints on subduction zone magmatism, *Earth Planet. Sci. Lett.*, *102*(3), 358–374.
McKenzie, D. P. (1969), Speculations on the consequences and causes of plate motions, *Geophys. J. Int.*, *18*(1), 1–32.
Morgan, J. P. (2001), Thermodynamics of pressure release melting of a veined plum pudding mantle, *Geochem. Geophys. Geosyst.*, *2*, 1001, doi:10.1029/2000GC000049.
Mullen, E. K., and D. Weis (2015), Evidence for trench-parallel mantle flow in the northern Cascade Arc from basalt geochemistry, *Earth Planet. Sci. Lett.*, *414*, 100–107.
Müller, R. D., M. Sdrolias, C. Gaina, and W. R. Roest (2008), Age, spreading rates and spreading asymmetry of the world's ocean crust, *Geochem. Geophys. Geosyst.*, *9*, Q04006, doi:10.1029/2007GC001743.

Nebel, O., and R. J. Arculus (2015), Selective ingress of a Samoan plume component into the northern Lau backarc basin, *Nat. Commun.*, *6*, Article 6554, doi:10.1038/ncomms7554.
Pacey, A., C. G. Macpherson, and K. J. McCaffrey (2013), Linear volcanic segments in the central Sunda Arc, Indonesia, identified using Hough transform analysis: implications for arc lithosphere control upon volcano distribution, *Earth Planet. Sci. Lett.*, *369*, 24–33.
Peacock, S. M. (1990), Fluid processes in subduction zones, *Science*, *248*(4953), 329–337.
Plank, T., and D. Forsyth (2016), Thermal structure and melting conditions in the mantle beneath the basin and range province from seismology and petrology, *Geochem. Geophys. Geosyst.*, *17*, 1312–1338, doi:10.1002/2015GC006205.
Plank, T., and C. H. Langmuir (1988), An evaluation of the global variations in the major element chemistry of arc basalts, *Earth Planet. Sci. Lett.*, *90*(4), 349–370.
Plank, T., L. B. Cooper, and C. E. Manning (2009), Emerging geothermometers for estimating slab surface temperatures, *Nat. Geosci.*, *2*(9), 611–615.
Plank, T., K. A. Kelley, M. M. Zimmer, E. H. Hauri, and P. J. Wallace (2013), Why do mafic arc magmas contain 4wt% water on average?, *Earth Planet. Sci. Lett.*, *364*, 168–179.
Ruscitto, D., P. Wallace, E. Johnson, A. Kent, and I. Bindeman (2010), Volatile contents of mafic magmas from cinder cones in the Central Oregon High Cascades: Implications for magma formation and mantle conditions in a hot arc, *Earth Planet. Sci. Lett.*, *298*(1), 153–161.
Rychert, C. A., K. M. Fischer, G. A. Abers, T. Plank, E. Syracuse, J. M. Protti, V. Gonzalez, and W. Strauch (2008), Strong along-arc variations in attenuation in the mantle wedge beneath Costa Rica and Nicaragua, *Geochem. Geophys. Geosyst.*, *9*, Q10S10, doi:10.1029/2008GC002040.
Schiano, P. (2003), Primitive mantle magmas recorded as silicate melt inclusions in igneous minerals, *Earth Sci. Rev.*, *63*(1), 121–144.
Schmidt, M., and S. Poli (2014), Devolatilization during subduction, in *The Crust, Treatise on Geochemistry*, edited by H. D. Holland and K. K. Turekian, 2nd ed., pp. 669–701, Elsevier, Oxford.
Schmidt, M. W., and S. Poli (1998), Experimentally based water budgets for dehydrating slabs and consequences for arc magma generation, *Earth Planet. Sci. Lett.*, *163*(1), 361–379.
Sdrolias, M., and R. D. Müller (2006), Controls on back-arc basin formation, *Geochem. Geophys. Geosyst.*, *7*, Q04,016, doi:10.1029/2005GC001090.
Shaw, A., E. Hauri, T. Fischer, D. Hilton, and K. Kelley (2008), Hydrogen isotopes in Mariana arc melt inclusions: Implications for subduction dehydration and the deep-earth water cycle, *Earth Planet. Sci. Lett.*, *275*(1), 138–145.
Sillitoe, R. H. (2010), Porphyry copper systems, *Econ. Geol.*, *105*(1), 3–41.
Sparks, D. W., and E. Parmentier (1991), Melt extraction from the mantle beneath spreading centers, *Earth Planet. Sci. Lett.*, *105*(4), 368–377.
Spiegelman, M., and D. McKenzie (1987), Simple 2-D models for melt extraction at mid-ocean ridges and island arcs, *Earth Planet. Sci. Lett.*, *83*(1), 137–152.
Stein, C. A., and S. Stein (1992), A model for the global variation in oceanic depth and heat flow with lithospheric age, *Nature*, *359*(6391), 123–129.
Syracuse, E. M., and G. A. Abers (2006), Global compilation of variations in slab depth beneath arc volcanoes and implications, *Geochem. Geophys. Geosyst.*, *7*, Q05017, doi:10.1029/2005GC001045.
Syracuse, E. M., P. E. van Keken, and G. A. Abers (2010), The global range of subduction zone thermal models, *Phys. Earth Planet. Inter.*, *183*(12), 73–90, doi:10.1016/j.pepi.2010.02.004.
Tatsumi, Y. (1986), Formation of the volcanic front in subduction zones, *Geophys. Res. Lett.*, *13*(8), 717–720.
Taylor, R. N., and R. W. Nesbitt (1998), Isotopic characteristics of subduction fluids in an intra-oceanic setting, Izu–Bonin Arc, Japan, *Earth Planet. Sci. Lett.*, *164*(1), 79–98.
Taylor, S. R., and S. M. McLennan (1995), The geochemical evolution of the continental crust, *Rev. Geophys.*, *33*(2), 241–265.
Turcotte, D. L., and G. Schubert (2014), *Geodynamics*, Cambridge Univ. Press, Cambridge, U. K.
Turner, S. J., and C. H. Langmuir (2015a), The global chemical systematics of arc front stratovolcanoes: Evaluating the role of crustal processes, *Earth Planet. Sci. Lett.*, *422*, 182–193, doi:10.1016/j.epsl.2015.03.056.
Turner, S. J., and C. H. Langmuir (2015b), What processes control the chemical compositions of arc front stratovolcanoes?, *Geochem. Geophys. Geosyst.*, *16*, 1865–1893, doi:10.1002/2014GC005633.
Turner, S. J., C. H. Langmuir, R. F. Katz, M. A. Dungan, and S. Escrig (2016), Parental arc magma compositions dominantly controlled by mantle-wedge thermal structure, *Nat. Geosci.*, *9*, 772–776.
van Keken, P. E., B. Kiefer, and S. M. Peacock (2002), High-resolution models of subduction zones: Implications for mineral dehydration reactions and the transport of water into the deep mantle, *Geochem. Geophys. Geosyst.*, *3*(10), 1056, doi:10.1029/2001GC000256.
van Keken, P. E., C. Currie, S. D. King, M. D. Behn, A. Cagnioncle, J. He, R. F. Katz, S.-C. Lin, E. M. Parmentier, M. Spiegelman, and K. Wang (2008), A community benchmark for subduction zone modeling, *Phys. Earth Planet. Inter.*, *171*, 187–197, doi:10.1016/j.pepi.2008.04.015.
van Keken, P. E., B. R. Hacker, E. M. Syracuse, and G. A. Abers (2011), Subduction factory: 4. Depth-dependent flux of H_2O from subducting slabs worldwide, *J. Geophys. Res.*, *116*, B01401, doi:10.1029/2010JB007922.
Wada, I., and K. Wang (2009), Common depth of slab-mantle decoupling: Reconciling diversity and uniformity of subduction zones, *Geochem. Geophys. Geosyst.*, *10*, Q10009, doi:10.1029/2009GC002570.
Wada, I., K. Wang, J. He, and R. D. Hyndman (2008), Weakening of the subduction interface and its effects on surface heat flow, slab dehydration, and mantle wedge serpentinization, *J. Geophys. Res.*, *113*, B04402, doi:10.1029/2007JB005190.
Wasylenki, L. E., M. B. Baker, A. J. Kent, and E. M. Stolper (2003), Near-solidus melting of the shallow upper mantle: Partial melting experiments on depleted peridotite, *J. Petrol.*, *44*(7), 1163–1191.
Watt, S. F., D. M. Pyle, T. A. Mather, and J. A. Naranjo (2013), Arc magma compositions controlled by linked thermal and chemical gradients above the subducting slab, *Geophys. Res. Lett.*, *40*, 2550–2556, doi:10.1002/grl.50513.
Weaver, S. L., P. J. Wallace, and A. D. Johnston (2011), A comparative study of continental vs. intraoceanic arc mantle melting: Experimentally determined phase relations of hydrous primitive melts, *Earth Planet. Sci. Lett.*, *308*(1), 97–106.
Wiens, D. A., K. A. Kelly, and T. Plank (2006), Mantle temperature variations beneath back-arc spreading centers inferred from seismology, petrology and bathymetry, *Earth Planet. Sci. Lett.*, *248*, 30–42, doi:10.1016/j.epsl.2006.04.011.
Wilkinson, J. J. (2013), Triggers for the formation of porphyry ore deposits in magmatic arcs, *Nat. Geosci.*, *6*(11), 917–925.
Wilson, C. R., M. Spiegelman, P. E. van Keken, and B. R. Hacker (2014), Fluid flow in subduction zones: The role of solid rheology and compaction pressure, *Earth Planet. Sci. Lett.*, *401*, 261–274.
Wirth, E. A., and J. Korenaga (2012), Small-scale convection in the subduction zone mantle wedge, *Earth Planet. Sci. Lett.*, *357*, 111–118.

Woodhead, J., S. Eggins, and J. Gamble (1993), High field strength and transition element systematics in island arc and back-arc basin basalts: Evidence for multi-phase melt extraction and a depleted mantle wedge, *Earth Planet. Sci. Lett.*, *114*(4), 491–504.

Zhang, Y., H. Ni, and Y. Chen (2010), Diffusion data in silicate melts, *Rev. Mineral. Geochem.*, *72*(1), 311–408.

Zhao, D., A. Hasegawa, and H. Kanamori (1994), Deep structure of Japan subduction zone as derived from local, regional, and teleseismic events, *J. Geophys. Res.*, *99*(B11), 22,313–22,329.

Zhao, D., Y. Xu, D. A. Wiens, L. Dorman, J. Hildebrand, and S. Webb (1997), Depth extent of the Lau back-arc spreading center and its relation to subduction processes, *Science*, *278*(5336), 254–257.